NeuroImage 200 (2019) 644–658

Contents lists available at ScienceDirect

NeuroImage

journal homepage: www.elsevier.com/locate/neuroimage

Neurovascular decoupling in type 2 diabetes mellitus without mild cognitive impairment: Potential biomarker for early cognitive impairment

Ying Yu [a,1], Lin-Feng Yan [a,1], Qian Sun [a,1], Bo Hu [a,1], Jin Zhang [a], Yang Yang [a], Yu-Jie Dai [b], Wu-Xun Cui [a], Si-Jie Xiu [a], Yu-Chuan Hu [a], Chun-Ni Heng [c], Qing-Quan Liu [c], Jun-Feng Hou [c], Yu-Yun Pan [d], Liang-Hao Zhai [d], Teng-Hui Han [d], Guang-Bin Cui [a,**], Wen Wang [a,*]

[a] Department of Radiology & Functional and Molecular Imaging Key Lab of Shaanxi Province, Tangdu Hospital, Fourth Military Medical University (Air Force Medical University), 569 Xinsi Road, Xi'an, 710038, Shaanxi, China
[b] Department of Clinical Nutrition, Xijing Hospital, Fourth Military Medical University (Air Force Medical University), 15 West Changle Road, Xi'an, 710032, Shaanxi, China
[c] Department of Endocrinology, Tangdu Hospital, Fourth Military Medical University (Air Force Medical University), 569 Xinsi Road, Xi'an, 710038, Shaanxi, China
[d] Student Brigade, Fourth Military Medical University (Air Force Medical University), 169 Changle Road, Xi'an, 710032, Shaanxi, China

ARTICLE INFO

Keywords:
Type 2 diabetes mellitus
Cognitive impairment
Neurovascular coupling
Default mode network
Executive function

ABSTRACT

Type 2 diabetes mellitus (T2DM) is a significant risk factor for mild cognitive impairment (MCI) and the acceleration of MCI to dementia. The high glucose level induce disturbance of neurovascular (NV) coupling is suggested to be one potential mechanism, however, the neuroimaging evidence is still lacking. To assess the NV decoupling pattern in early diabetic status, 33 T2DM without MCI patients and 33 healthy control subjects were prospectively enrolled. Then, they underwent resting state functional MRI and arterial spin labeling imaging to explore the hub-based networks and to estimate the coupling of voxel-wise cerebral blood flow (CBF)-degree centrality (DC), CBF-mean amplitude of low-frequency fluctuation (mALFF) and CBF- mean regional homogeneity (mReHo). We further evaluated the relationship between NV coupling pattern and cognitive performance (false discovery rate corrected). T2DM without MCI patients displayed significant decrease in the absolute CBF-mALFF, CBF-mReHo coupling of CBFnetwork and in the CBF-DC coupling of DCnetwork. Besides, networks which involved CBF and DC hubs mainly located in the default mode network (DMN). Furthermore, less severe disease and better cognitive performance in T2DM patients were significantly correlated with higher coupling of CBF-DC, CBF-mALFF or CBF-mReHo, especially for the cognitive dimensions of general function and executive function. Thus, coupling of CBF-DC, CBF-mALFF and CBF-mReHo may serve as promising indicators to reflect NV coupling state and to explain the T2DM related early cognitive impairment.

1. Introduction

Type 2 diabetes mellitus (T2DM) is a significant risk factor for mild cognitive impairment (MCI). Once MCI occurs, it progresses to dementia at an annual rate of 8.43% (Roberts et al., 2014; Ma et al., 2015; Xu et al., 2010; Pal et al., 2018). Though the cognitive function remains "normal" for a long period before MCI, many subitems of cognitive dimensions have already been gradually impaired during this period (Ma et al., 2015; Yang et al., 2018). To prevent T2DM patients from developing MCI, it's essential to explore the neuropathological mechanism of cognitive alterations, and to screen the imaging biomarkers for early intervention at the pre-MCI stage (T2DM patients without MCI).

Tentative explorations on cerebral impairment in T2DM without MCI patients have been performed using functional magnetic resonance imaging (fMRI). Significant structural and iron metabolism disruptions have

* Corresponding author.
** Corresponding author.
E-mail addresses: yytdfsk@fmmu.edu.cn (Y. Yu), yanlinfeng@fmmu.edu.cn (L.-F. Yan), sunqian0319@163.com (Q. Sun), rayhb@foxmail.com (B. Hu), 517988152@qq.com (J. Zhang), yyang507@126.com (Y. Yang), daiyujie1222@qq.com (Y.-J. Dai), cuiwuxun@163.com (W.-X. Cui), 314274263@qq.com (S.-J. Xiu), hyc3140@126.com (Y.-C. Hu), lvchenyeye@126.com (C.-N. Heng), liuqingq@gmail.com (Q.-Q. Liu), houjf119@fmmu.edu.cn (J.-F. Hou), panyuyun1997@163.com (Y.-Y. Pan), 1074252572@qq.com (L.-H. Zhai), hantenghui678@163.com (T.-H. Han), cuigbtd@fmmu.edu.cn (G.-B. Cui), wangwen@fmmu.edu.cn (W. Wang).
[1] These authors contributed equally to this work.

https://doi.org/10.1016/j.neuroimage.2019.06.058
Received 10 January 2019; Received in revised form 22 June 2019; Accepted 24 June 2019
Available online 25 June 2019
1053-8119/© 2019 Elsevier Inc. All rights reserved.

Abbreviation

T2DM	type 2 diabetes mellitus
HC	healthy control
CBF	cerebral blood flow
FC	functional connectivity
NV	neurovascular
DC	degree centrality
mALFF	mean amplitude of low-frequency fluctuation
mReHo	mean regional homogeneity
DMN	default mode network
3D-pCASL	three-dimensional pseudo-continuous arterial spin labeling
3D-BRAVO	three-dimensional brain volume imaging
TE	echo time
TR	repetition time
VBM	voxel-based morphometry
FWHM	full width at half maximum
HbA1c	glycosylated hemoglobin A1c
FBG	fasting blood glucose
BMI	body mass index
SP	systolic pressure
DP	diastolic pressure
HDL	high density lipoprotein
LDL	low density lipoprotein
MMSE	mini-mental state examination
MoCA	Montreal cognitive assessment
SAS	self-rating anxiety scale
SDS	self-rating depression scale
GM	gray matter
WM	white matter
CSF	cerebrospinal fluid
MCI	mild cognitive impairment
CA	correct answers
EA	errors answers
MA	missed answers
CGRT	congruent reaction time
ICRT	incongruent reaction time
NRT	neutral reaction time
CRT	color reaction time
CGCR	congruent correct response
ICT	incongruent correct response
NCR	neutral correct response
CCR	color correct response
Cb_Right_X	cerebellar lobule X, right
INS_R_6_5	dorsal granular insula, right
STG_L_6_3	superior temporal gyrus, part 3 (area TE), left
PoG_L_4_1	postcentral gyrus, part 1 (area 1/2/3 upper limb), left
MFG_L_7_4	middle frontal gyrus, part 4 (ventral area 9/46), left
PCun_R_4_1	precuneus, part 1 (medial area 7), right
STG_R_6_4	superior temporal gyrus, part 4 (caudal area 22), right
IPL_R_6_3	inferior parietal lobule, part 3 (rostrodorsal area 40), right
pSTS_L_2_1	posterior superior temporal sulcus, part 1 (rostroposterior superior temporal sulcus), left
pSTS_R_2_1	posterior superior temporal sulcus, part 1 (rostroposterior superior temporal sulcus), right
PoG_R_4_4 (1/2/3t)	postcentral gyrus, part 4 (area1/2/3 trunk), right
FDR	false discovery rate
GRF	gaussian random field

already been found in extensive regions at pre-MCI stage (Yang et al., 2018; Zhang et al., 2014; Sun et al., 2018). We also demonstrated that the structural disruptions were closely associated with hippocampal functional connectivity (FC) in T2DM without MCI patients (Sun et al., 2018). However, the putative functional consequences of these observed structural alterations remain unclear.

Previous functional imaging studies on T2DM mainly focused on cerebral perfusion or neural activity (Cui et al., 2014, 2017; Last et al., 2007; Dai et al., 2017; Peng et al., 2016; Zhou et al., 2014). However, the altered cerebral blood flow (CBF) and spontaneous neural activities (including degree centrality (DC), mean amplitude of low-frequency fluctuation (mALFF) and mean regional homogeneity (mReHo)) do not always match in T2DM patients (Dai et al., 2017; Cui et al., 2014; Peng et al., 2016; Jansen et al., 2016; Liu et al., 2018). The spatial inconsistency between altered cerebral perfusion and neural activities makes it difficult to figure out the mechanism underlying the diabetic cognitive impairment.

As is well-appreciated, there is a tight coupling between the blood supply and the brain function in healthy adults, i.e. the neurovascular (NV) coupling that is the physiological basis for human brainnetome (Liang et al., 2013; Del Zoppo, 2013; Muoio et al., 2014). The NV decoupling is suggested to play an important role in the MCI and Alzheimer's disease (Nelson et al., 2016; Iadecola, 2017). Furthermore, recent animal studies have shown that NV decoupling occurs at the early stage of T2DM and plays a crucial role in the transformation from diabetes-related cognitive impairments to Alzheimer's disease (Shekhar et al., 2017; Duarte et al., 2015; Mogi and Horiuchi, 2011; Bae et al., 2011; Beauquis et al., 2010). Thus, NV coupling may be a promising imaging biomarker to explore critical brain regions or networks for early intervention at the pre-MCI stage (Iadecola, 2017).

According to prior studies, the CBF-DC coupling was used to characterize the coupling between vascular perfusion and spontaneous neural activity, which cannot be achieved by investigating the CBF or neural activity indicators alone (Liang et al., 2013; Zhu et al., 2017; Sheng et al., 2018; Khalili-Mahani et al., 2014). NV decoupling was found in patients with major depressive disorder and schizophrenia, and was proved to be a possible neuropathological mechanism for brain dysfunction (Zhu et al., 2017; Sheng et al., 2018). However, in T2DM without MCI patients, it is still unclear what the NV coupling pattern is and what is its contribution to cognitive function. Besides, it is not clear which cognitive dimension is most vulnerable in T2DM without MCI patients. We have preliminarily explored the regional alterations of CBF-DC and CBF-ALFF coupling in T2DM (Hu et al., 2019). NV biomarkers in T2DM patients were significantly decreased in 10 brain regions, indicating correlations between neuronal activity and cerebral perfusion maps to be a feasibility method for detecting NV coupling abnormalities. However, the cognitive function state of the recruited patients was heterogeneous in the previous study. Besides, functional networks are the basis for the organizing and segregating higher-level functional information (Chen et al., 2016a). Considering that the regions with altered CBF and DC to be the functional hubs for the whole brain (Li et al., 2016; Cui et al., 2017; Shen et al., 2015; Liang et al., 2014; Liska et al., 2015) and be firstly impaired, leading to the deterioration of disease (Gibas, 2017), networks of regions with altered CBF or DC may play a key role in the early cognitive impairment in T2DM (Cui et al., 2016; Xie et al., 2015). Thus, in the current study, we recruited T2DM without MCI patients and further explored the NV coupling pattern in the hub-based network. The relationship between NV indicators and cognitive function was assessed as well.

We hypothesized that the slight cognitive alteration and the mismatch of CBF and DC alterations have already existed in T2DM without MCI patients. The hub-based networks mainly locate in the default mode network (DMN) and the NV decoupling of these networks and regions contributes to cognitive impairment at the pre-MCI stage. To

address these issues, we firstly collected resting-state fMRI (rs-fMRI) and three-dimensional pseudo-continuous arterial spin labeling (3D-pCASL) data to identify T2DM-related hubs. Then we explored the voxel-wise coupling of CBF-DC, CBF-mALFF and CBF-mReHo within the networks constructed with the altered CBF or DC regions. We further investigated the relationship between NV coupling alteration and cognitive performance. The final goal of this study is to assess the altered NV coupling pattern that plays an important role in early diabetic cognitive impairment.

2. Material and methods

2.1. Standard protocol approval, registration, and patient consents

This study has been approved by the "Ethics Committee of Tangdu Hospital" (2014-03-03) and been registered to ClinicalTrials.gov (NCT02420470, https://www.clinicaltrials.gov/). Written informed consents were obtained after a full description of the study to all participants. All the experiments were conducted according to the principles expressed in the Declaration of Helsinki. The datasets used or analyzed during the current study are available from the corresponding author upon reasonable request.

2.2. Participants

T2DM patients, Chinese Han and right-handed, were recruited from inpatients and outpatients in Tangdu Hospital from October 21, 2016, to December 1, 2017. Matched healthy control (HC) subjects were recruited from the local community or the physical examination center in Tangdu Hospital during the same period. Fasting blood glucose (FBG) test and/or oral glucose tolerance test (OGTT) were conducted. Then, matched T2DM without MCI patients and HC participants were defined according to the general cognitive impairment screening by Mini-Mental State examination (MMSE) and Montreal Cognitive Assessment (MoCA).

The diabetic patients were all previously diagnosed with T2DM, except for two subjects who were initially recruited as control subjects but with FPG exceeding 7 mmol/L. Diagnosis of T2DM was based on the latest criteria of American Diabetes Association (American Diabetes, 2014). Considering that hyperglycemia plays a key role in diabetic cognitive impairment, diabetic subjects with normal HbA1c were excluded (Cerasuolo and Izzo, 2017). Individuals with no evidence of T2DM were recruited into HC group. Their FPG levels were <5.6 mmol/L, and 2-h fasting glucose levels for OGTT were <7.8 mmol/L. All the participants were between 35 and 70 (mean $\pm$ SD, 52.26 ± 7.43) years old. None of the T2DM patients had retinopathy or neuropathy.

Subjects who met any of the exclusion criteria were excluded: 1) MMSE score <27; 2) MoCA score <24; 3) foreign metal in or around their body; 4) Subjects with pregnancy and claustrophobia; 5) history of serious brain diseases (significant brain trauma, tumor, stroke, meningitis, cerebral infarction) or myocardial infarction; 6) central nervous system neurological disorder, or medical illness significantly affecting neurological function; 7) individuals who took psychoactive or steroid hormones drugs within 3 months; 8) left-handedness and ambidexterity (determined by the Edinburgh Handedness Inventory); 9) body mass index (BMI) $\geq 35\ kg/m^2$; 10) poor image quality or excessive head movement (translation >3.0 mm or rotation $>3^\circ$). Two T2DM patients with severe white matter hyperintensity were excluded according to the conventional images reviewed by a senior radiologist. Four T2DM patients and one HC subject were excluded because of excessive head movement during fMRI runs. One T2DM patient and one HC subject were excluded for incomplete image scanning. Another two T2DM patients were excluded because of significant cognitive impairment. Finally, a total of 33 T2DM without MCI patients and 33 sex- and age-matched healthy subjects were recruited for the present study.

2.3. Demographic, clinical characteristics and cognitive assessment

Demographic and clinical characteristics were recorded, including age, gender, years of education, months since T2DM was diagnosed, blood pressure (BP), BMI, FBG, HbA1c, total cholesterol, triglyceride, low-density lipoprotein (LDL) cholesterol and high-density lipoprotein (HDL) cholesterol.

All participants completed the MMSE, the MoCA, Self-Rating Anxiety Scale (SAS), Self-rating depression scale (SDS), the Stroop Color-Word Test (SCWT), and the California Verbal Learning Test (CVLT). This battery of psychological assessment mainly assesses general cognitive capability, state of anxiety and depression, executive function, and memory function, respectively.

2.4. MRI acquisition

Within 2 h after the cognitive assessment, MRIs were acquired using a 3.0-T MRI system (MR750; GE Healthcare, Milwaukee, WI, USA) with an 8-channel head coil array. Foam paddings were used to restrict the head motion. All participants were screened for foreign metal in or around their body before scanning. All procedures of image analysis were blinded to grouping situation. All of the imaging results were interpreted in the Human Brainnetome Atlas (BNA, https://scalablebrainatlas.incf.org/human/BNA) (Fan et al., 2016).

2.4.1. Conventional protocols

Volumetric T1-weighted (three-dimensional brain volume imaging, 3D-BRAVO) (echo time (TE)/repetition time (TR) = 3.2/8.2 ms, inversion time (TI) = 450 ms, flip angle (FA) = 12°, acquisition matrix = 256 × 256, slice thickness = 1 mm, slice number = 188) images were collected for the assessment of brain volume. Clinical T1 weighted images, T2 weighted images, T2 fluid attenuated inversion recovery (FLAIR) images (TE/TR = 149/8400 ms, TI = 2100 ms, FA = 111°, acquisition matrix = 256 × 256, reconstruction matrix = 512 × 512, slice thickness = 5 mm, gap = 6.5 mm) and Time-of-flight magnetic resonance angiography (TOF-MRA) (TE/TR = 3.4/25 ms, FA = 20°, acquisition matrix = 320 × 224, reconstruction matrix = 512 × 512, slice thickness = 1.4 mm, gap = 0.7 mm) were obtained for the assessment of white matter hyperintensity and other intracranial lesions.

2.4.2. 3D-pCASL images

According to the White Paper of the International Society for Magnetic Resonance in Medicine (ISMRM) perfusion study group (Alsop et al., 2015; van Osch et al., 2018), perfusion images were obtained using a 3D-pCASL technique with the following parameters: slice = 50, TR = 5046 ms, post label delay (PLD) = 2025 ms, TE = 11 ms, slice thickness = 3 mm, FA = 111°, field of view = 256 × 256 mm, acquisition matrix = 128 × 128, the bottom of the slab should be positioned at the bottom of the cerebellum, with coverage of the entire cerebrum. The whole scanning time is 4 min.

2.4.3. rs-fMRI

rs-fMRI parameters included gradient-echo planar sequence sensitive to BOLD contrast (TR = 2000 ms, TE = 30 ms, FA = 90°), whole-brain volumes with 36 contiguous 3-mm-thick transverse slices, no interstices gap, and 3 mm × 3 mm two-dimensional resolution. Patients were required to lie still in the scanner with their eyes closed but remain awake just before rs-fMRI scanning. After rs-fMRI scanning, they were asked to ensure if they were awake during scanning.

2.5. Functional imaging analysis

2.5.1. Structural preprocessing

Voxel-based morphometry (VBM) analysis was implemented via statistical parametric mapping (SPM8) (http://www.fil.ion.ucl.ac.uk/spm/software/spm8/), in conjunction with DARTEL and vbm8

toolbox. All 3D-BRAVO images were checked to exclude artifacts and gross anatomical abnormalities. All images were spatially normalized into the identical Montreal Neurological Institute (MNI) coordinate system. Then, the standardized structural images were segmented into gray matter (GM), white matter (WM) and cerebrospinal fluid (CSF) using the new Segment and Dartel modules in SPM8. The segmented, modulated GM images were smoothed with an 8-mm full-width at half-maximum (FWHM) isotropic Gaussian kernel. Global volumes of GM, WM and CSF were calculated from the modulated normalized segmented images.

2.5.2. 3D-pCASL analysis

Data was preprocessed using SPM8, in which 3D-BRAVO and 3D-pCASL images were corrected for gradient nonlinearities in all directions. Realignment, coregistration and segmentation were included in the preprocessing. ASL images were registered to the brain extracted from the 3D-BRAVO. Mean whole-brain CBF values were calculated in the mask, and converted to quantitative CBF maps with the unit of mL/100 g/min. And then they were normalized to Montreal Neurological Institute (MNI) space with a 3-mm isotropic resolution, and smoothed with an isotropic kernel of 8 mm. One-sample *t*-test was performed in T2DM or HC group to explore the perfusion distribution ($p < 0.05$, corrected with gaussian random field (GRF)).

2.5.3. rs-fMRI data preprocessing

rs-fMRI imaging data was preprocessed in Data Processing Assistant for Resting-State fMRI (DPABI, http://www.restfmri.net/forum/DPARSF) (Yan et al., 2016) and the SPM8 software package in MATLAB R2012b platform. The first 10 time points were discarded. Slice timing and realignment for head motion correction were performed. Any images with head motion at 3.0-mm translation or 3.0° rotation in any direction were excluded. Then, detrending was carried out. Possible contaminations from the signals in WM, GM and CSF, and 24-motion vectors were regressed out from the whole brain (Chen et al., 2012). Then, a bandpass filter was applied to keep only low-frequency fluctuations within the frequency range of 0.01 and 0.1 Hz.

2.5.4. Gray matter DC analysis

For each subject, the DC value was calculated for each voxel. We computed Pearson's correlation coefficients between the BOLD time courses of all pairs of voxels within the Brain mask. Then the brain functional connectivity matrix of each participant was analyzed. Meanwhile, we removed the global signal and restricted our analysis to positive correlations above a threshold of 0.2 to eliminate weak correlations. The correlation coefficients over the threshold were averaged over the whole brain mask. And then, the mean value was stored back in the certain voxel. The whole process was repeated for all other voxels. The DC maps were smoothed with an 8 mm FWHM Gaussian kernel. To find the between-group difference, two-sample voxel-wise *t*-test was performed ($p < 0.05$, corrected with GRF). Seed-based functional connectivity (FC) was calculated as well. Detailed FC analysis process and results were described in the Supplementary material.

2.5.5. mALFF and mReHo analysis

The mALFF and mReHo values were both calculated using REST (REST1.8; http://www.restfmri.net).The ALFF is the averaged square root of the power spectrum via fast Fourier transform (FFT) across a 0.01–0.1 Hz window at each voxel. mALFF reflected the degree of its raw ALFF value relative to the averaged ALFF value of the whole brain. After filtering in data preprocessing, ReHo values were quantified by calculating Kendall coefficient of concordance (KCC) between a given voxel and its neighbors in a voxel-wise way (Li et al., 2018a). mReHo reflected the degree of its raw ReHo value relative to the averaged ReHo value of the whole brain. Finally, the mReHo were spatially smoothed with the Gaussian kernel (8 mm FWHM). In each participant, mALFF and mReHo of the regions with altered CBF and DC values were extracted to explore the between-group difference.

2.5.6. Whole brain-based, network-based and regional based NV coupling

We constructed the hub-based networks as "CBFnetwork" or "DCnetwork", which included the regions with altered CBF or DC values, respectively. Regional DC, mALFF and mReHo within CBFnetwork or DCnetwork were calculated and normalized into z-scores, respectively. To quantitatively evaluate the coupling between CBF and the neural activity indicators, the CBF, DC, mALFF, mReHo values of each voxel were extracted. For each individual, 3 whole GM neurovascular biomarkers were firstly assessed by Pearson correlation analysis, i.e. coupling coefficients of CBF-DC, CBF-mALFF and CBF-mReHo. The correlation coefficients of each networks and the regions in them were also analyzed as described in previous studies (Zhu et al., 2017; Sheng et al., 2018; Hu et al., 2019). In order to investigate the comprehensive cross-modality relationship among CBF, DC, mALFF, mReHo values in each network and to explore whether there is a between-group difference, the mean values of these matrics at network or regional level were extracted in each individual. These mean values were imported into R (R version 3.6.0, https://www.r-project.org/) to construct the cross-modality correlation matrix. Correlation coefficients of each pair in two groups were extracted as paired samples for the further group-difference comparison of CBF/DC/mALFF/mReHo correlation matrix (Aiello et al., 2015).

To test the patterns mALFF and mReHo changes underlying cognitive impairment in T2DM patients, we also used the regions with altered mALFF or mReHo to construct "mALFFnetwork" or "mReHonetwork". The network-based and regional based CBF-DC, CBF-mALFF and CBF-mReHo correlation coefficients and CBF/DC/mALFF/mReHo matrix correlation coefficients were calculated as how these measurements were analyzed in CBFnetwork.

2.6. Statistical analysis

2.6.1. Group difference of demographic, clinical, brain volume, cognitive variables

Group differences of demographic, clinical, global mean GM, WM and CSF volume, and cognitive variables involving continuous data were analyzed with Student *t*-test or Mann-Whitney *U* test. Difference in gender was analyzed using *chi-square* test. Z scores of each cognitive test and image features for each subject were converted from the raw data with reference to the means and standard deviations of all subjects.

2.6.2. Voxel-wise group analyses

Voxel-wise group comparisons of GM, WM and CSF volume, CBF, DC maps were performed using two sample *t*-test in SPM8 with age, gender, BMI, years of education as covariates while GM volume (GMV) was an additional covariate in the comparisons of CBF, DC. Results were corrected for multiple comparisons using voxel-based GRF ($p < 0.05$) which was implemented in REST on the MATLAB R2012b platform (Yuan et al., 2016; Li et al., 2018b). Considering that atrophy may cause local changes in NV coupling, we repeated the above-mentioned analyses without GMV regression.

2.6.3. Group difference of NV coupling and correlation analysis

Two-sample *t*-test was implemented to test the group differences of regional mALFF, regional mReHo, coupling coefficients of CBF-DC, CBF-mALFF and CBF-mReHo at the global level, network level and region level, respectively. Group difference of the CBF/DC/mALFF/mReHo matrix correlation coefficient was tested by paired-samples *t*-test. Then in T2DM group, linear correlation analysis was performed to explore the relationship between the significant altered coupling of CBF-DC, CBF-mALFF and CBF-mReHo in all networks and cognitive scores with significant group differences. In addition, correlations between these imaging features and T2DM severity-related clinical indicators (i.e., FBG, HbA1c, disease duration) were analyzed. The correlation coefficients were also tested between CBF, DC, mALFF, mReHo and cognitive performance at the regional level and network level. False discovery rate

(FDR) method in R (v3.5.3) was used for the multiple comparison correction of coupling coefficients of CBF-DC, CBF-mALFF and CBF-mReHo comparison and the correlation analysis. Significant levels were set at $p < 0.05$ after FDR correction.

3. Results

3.1. Demographic, clinical, cognitive results

Clinical and demographic characteristics for T2DM without MCI and HC groups were summarized in Table 1. There was no significant intergroup difference in age, gender distribution, education level, BMI, blood pressure, triglycerides, total cholesterol, HDL, LDL, total score of MMSE, MoCA, SAS, SDS. Higher levels of FBG ($P = 0.002$), HbA1c ($P < 0.001$) were found. According to Table 2, poorer performance was found in T2DM in 3 subitems of SCWT, i.e. missed answers (MA) ($P = 0.036$), neutral reaction time (NRT) ($P = 0.022$), neutral correct response (NCR) ($P = 0.025$). Furthermore, poorer performance was found in T2DM patients in 6 subitems of CVLT, i.e. trial 4 ($P = 0.009$), short-delay free recall ($P = 0.008$), short-delay cued recall ($P = 0.003$), free recall intrusions ($P = 0.012$), cued recall intrusions ($P = 0.017$), total intrusions ($P = 0.008$).

3.2. Brain volume

Global MRI metrics are presented in Table 1. After accounting for age, sex, BMI and education level, no difference in global mean GM, WM and CSF volume was observed between groups. Furthermore, in terms of voxel-wise comparison, no significant region was observed after GRF correction.

Table 1
Demographic and clinical characteristics of the subjects.

Characteristics	T2DM without MCI (n = 33)	HC (n = 33)	P value
Age (years)	53.45(8.4)	51.00(5.3)	0.16
Gender, n (%)			0.09
Female	5(15)	11(33)	
Male	28(85)	22(67)	
Education (years)	12.75(2.44)	12.91(3.46)	0.84
T2DM duration (months)	85.12(62.40)	–	–
HbA1c (%)	8.12(1.73)	5.58(0.34)	0.00**
HbA1c (mmol/mol)	65.21(18.90)	38.70(3.58)	0.00**
FBG (mg/dL)	7.42(3.12)	5.60(0.59)	0.00*
BMI (kg/m2)	25.02(2.34)	23.99(2.12)	0.08
Blood pressure(mmHg)			
SP	127 (12)	126 (17)	0.86
DP	75 (15)	81(13)	0.11
Cholesterol(mg/dL)			
Total cholesterol	4.08(1.29)	4.32(0.60)	0.36
HDL cholesterol	0.91(0.40)	0.98(0.17)	0.41
LDL cholesterol	2.38(0.80)	2.72(0.50)	0.07
Triglycerides(mg/dL)	2.08(1.75)	2.35(1.45)	0.48
MMSE	28.94(0.93)	28.50(1.11)	0.09
MoCA	26.47(2.10)	26.77(2.02)	0.48
SAS	42.42(6.98)	40.75(7.12)	0.34
SDS	45.52(6.98)	43.22(10.79)	0.31
GM volume(m^3)	664.63(47.71)	672.14(55.61)	0.56
WM volume(m^3)	524.83(56.24)	508.98(69.17)	0.31
CSF(m^3)	252.11(35.87)	242.48(36.44)	0.28

Data are presented as mean (SD), or percentages. Abbreviation: T2DM, type 2 diabetes mellitus; HC, healthy control; HbA1c, glycosylated hemoglobin A1c; FBG, fasting blood glucose; BMI, body mass index; SP, systolic pressure; DP, diastolic pressure; HDL, high density lipoprotein; LDL, low density lipoprotein; MMSE, mini-mental state examination; MoCA, Montreal cognitive assessment; SAS, self-rating anxiety scale; SDS, self-rating depression scale; GM, gray matter; WM, white matter; CSF, cerebrospinal fluid. **, $P < 0.001$; *, $P < 0.05$.

Table 2
Neuropsychological performance of the subjects.

Characteristics	T2DM without MCI (n = 33)	HC (n = 33)	P value
Stroop color-word test (SCWT)			
Total score (z transformed)	−1.36(4.71)	−1.50(7.91)	0.96
CA(n)	31.56(11.21)	37.72(17.14)	0.11
EA(n)	39.75(11.52)	41.31(13.76)	0.63
MA(n)	49.44(14.64)	41.59(13.89)	0.04*
CGRT(ms)	216.44(114.00)	214.34(178.38)	0.51
ICRT(ms)	535.00(300.80)	616.03(375.45)	0.35
NRT(ms)	317.22(207.25)	486.21(329.06)	0.02*
CRT(ms)	132.56(93.15)	198.48(176.93)	0.08
CGCR(n)	5.43(2.50)	5.90(3.66)	0.57
ICT(n)	14.28(6.35)	15.62(6.94)	0.43
NCR(n)	8.47(4.06)	11.62(6.22)	0.02*
CCR(n)	3.5(1.85)	4.7(3.4)	0.09
California Verbal Learning Test (CVLT)			
Total score (z transformed)	−2.28(10.09)	1.84(8.20)	0.10
Trial 1(n)	4.72(2.19)	5.39(1.82)	0.22
Trial 2(n)	7.88(2.95)	8.00(2.19)	0.86
Trial 3(n)	9.52(2.80)	10.68(2.45)	0.11
Trial 4(n)	9.96(2.76)	11.77(2.23)	0.01*
Trial 5(n)	11.04(2.89)	12.39(2.39)	0.06
Total trials 1–5(n)	43.12(11.98)	46.97(11.69)	0.23
Trial B(n)	4.79(1.98)	5.87(2.66)	0.10
Short-delay free recall(n)	7.21(3.32)	9.68(3.28)	0.01*
Short-delay cued recall(n)	8.54(1.96)	10.39(2.35)	0.00*
Long-delay free recall(n)	8.46(2.92)	10.03(2.90)	0.05
Long-delay cued recall(n)	8.92(2.36)	10.23(2.75)	0.07
Free recall intrusions(n)	6.83(5.14)	3.65(3.95)	0.01*
Cued recall intrusions(n)	4.46(3.31)	2.23(3.07)	0.02*
Total intrusions(n)	11.29(7.83)	5.97(6.47)	0.01*
Total repetitions(n)	5.29(4.06)	5.84(5.18)	0.67
Forced-choice recognition(n)	98.70(2.59)	93.21(24.68)	0.28

Data are presented as mean (SD), or percentages. Abbreviation: T2DM, type 2 diabetes mellitus; HC, healthy control; MCI, mild cognitive impairment; CA, correct answers; EA, errors answers; MA, missed answers; CGRT, congruent reaction time; ICRT, incongruent reaction time; NRT, neutral reaction time; CRT, color reaction time; CGCR, congruent correct response; ICT, incongruent correct response; NCR, neutral correct response; CCR, color correct response. **, $P < 0.001$; *, $P < 0.05$.

3.3. Similar intergroup spatial patterns of the CBF, DC, mALFF and mReHo

T2DM patients and HC subjects exhibited similar spatial distributions of CBF, DC, mALFF and mReHo (Fig. 1A–B and Fig. 2A–B). Brain regions with higher CBF were mostly located in the posterior cingulate cortex/precuneus, anterior cingulate cortex, middle frontal gyrus, lateral temporal cortices, and superior temporal gyrus. Most of these regions are the main components of the DMN. Brain regions with higher DC were primarily distributed in lateral middle frontal gyrus, occipital gyrus, postcentral gyrus, inferior temporal gyrus, fusiform gyrus, thalamus, and striatum. Brain regions with higher mALFF were primarily distributed in bilateral supramarginal gyrus, prefrontal lobe, inferior temporal gyrus, superior frontal gyrus, posterior cingulate cortex, parahippocampal gyrus. Brain regions with higher mReHo were primarily distributed in bilateral parietal lobe, middle frontal gyrus, posterior cingulate cortex/precuneus, parahippocampal gyrus. As is shown in Figs. S1A–B and Figs. S2A–B of the Supplementary material, similar pattern of the spatial distributions of CBF, DC, mALFF and mReHo was observed in the process without GMV regression.

3.4. CBF, DC, mALFF and mReHo alterations between groups

Compared with HC subjects, T2DM patients showed significant

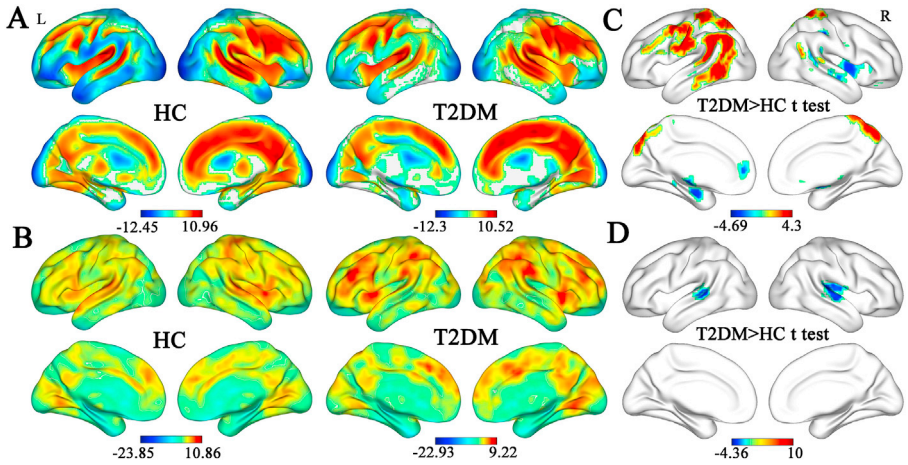

Fig. 1. Spatial distribution maps and the between-group differences of CBF and DC maps. One-sample *t*-test was performed in CBF (A) and DC (B) images in the two groups respectively. Under the between-group "T2DM > HC" *t*-test, intergroup differences of CBF and DC values were shown in (C) and (D) respectively (GRF corrected, $p < 0.05$).

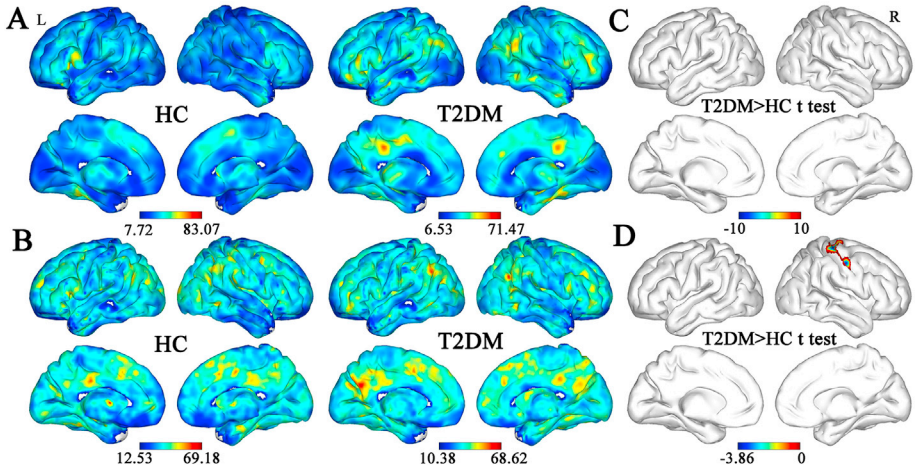

Fig. 2. Spatial distribution maps and the between-group differences of mALFF and mReHo maps. One-sample *t*-test was performed in mALFF (A) and mReHo (B) images in the two groups respectively. Under the between-group "T2DM > HC" *t*-test, intergroup differences of mALFF and mReHo values were shown in (C) and (D) respectively (GRF corrected, $p < 0.05$). No region with significantly altered mALFF value was found between groups. mReHo value in part 4 of right postcentral gyrus (PoG_R_4_4 (1/2/3t)) was significantly decreased in T2DM group compared to HC group.

decreased CBF in the right cerebellar lobule X (Cb_Right_X), right dorsal granular insula (INS_R_6_5), part 3 of left superior temporal gyrus (STG_L_6_3), left ventral area in middle frontal gyrus (MFG_L_7_4), part 3 of right inferior parietal lobule (IPL_R_6_3) and increased CBF in the left area 1/2/3 upper limb in postcentral gyrus (PoG_L_4_1), right medial area 7 in precuneus (PCun_R_4_1), part 4 of right superior temporal gyrus (STG_R_6_4). T2DM patients exhibited decreased DC in left rostroposterior superior temporal sulcus (pSTS_L_2_1) and in right rostroposterior superior temporal sulcus (pSTS_L_2_1) (Fig. 1C and Table S1 in the Supplementary material). T2DM patients exhibited decreased mReHo value in part 4 of right postcentral gyrus (PoG_R_4_4 (1/2/3t)) (Fig. 2C and Table S1 in the Supplementary material). However, no region with significantly altered mALFF value was found between groups.

In the process without GMV regression, most significant altered regions are the same as the results reported above except for the absence of IPL_R_6_3, STG_R_6_4 in CBF alterations and pSTS_L_2_1 in DC alterations. (Figs. S1C and S2C and Table S2 in the Supplementary material).

3.5. mALFF and mReHo changes in the CBF and DC network

As compared to HCs, no matter whether regress GMV, T2DM patients showed lower regional mALFF and mReHo values only in regions with altered DC, i.e. DCnetwork ($P_{mALFF}<0.001$, $P_{mReHo}<0.001$), pSTS_L_2_1 ($P_{mALFF}=0.001$, $P_{mReHo}=0.014$), pSTS_R_2_1 ($P_{mALFF}=0.003$, $P_{mReHo}<0.001$) in process regressed GMV (Fig. 3A) and pSTS_R_2_1 ($P_{mALFF}=0.021$, $P_{mReHo}=0.006$) in process without GMV regression (Fig. 3B).

3.6. Global, network, and regional coupling of CBF-DC, CBF-mALFF and CBF-mReHo

At the global level, CBF were significantly correlated with DC, mALFF and mReHo in both groups as is shown in Fig. 4. No significant difference was found between T2DM and HC groups in CBF-DC coupling coefficient ($rDM = 0.06 \pm 0.03$, $rHC = 0.05 \pm 0.03$, $P = 0.212$), CBF-mALFF coupling coefficient ($rDM = 0.83 \pm 0.04$, $rHC = 0.82 \pm 0.03$, $P = 0.132$), CBF-mReHo coupling coefficient ($rDM = 0.88 \pm 0.03$, $rHC = 0.87 \pm 0.02$, $P = 0.160$).

For CBFnetwork, CBF-mALFF ($P_{FDR} = 0.001$) and CBF-mReHo coupling ($P_{FDR} = 0.002$) in T2DM group were found to be higher than HC group, while no significant CBF-DC coupling was found between groups ($P_{FDR} = 0.168$) (Fig. 5C and Table 3). However, for DCnetwork, lower CBF-DC coupling was found in T2DM group comparing to that in HC group ($P_{FDR,}$ <0.001) (Fig. 5D and Table 3), while no significant

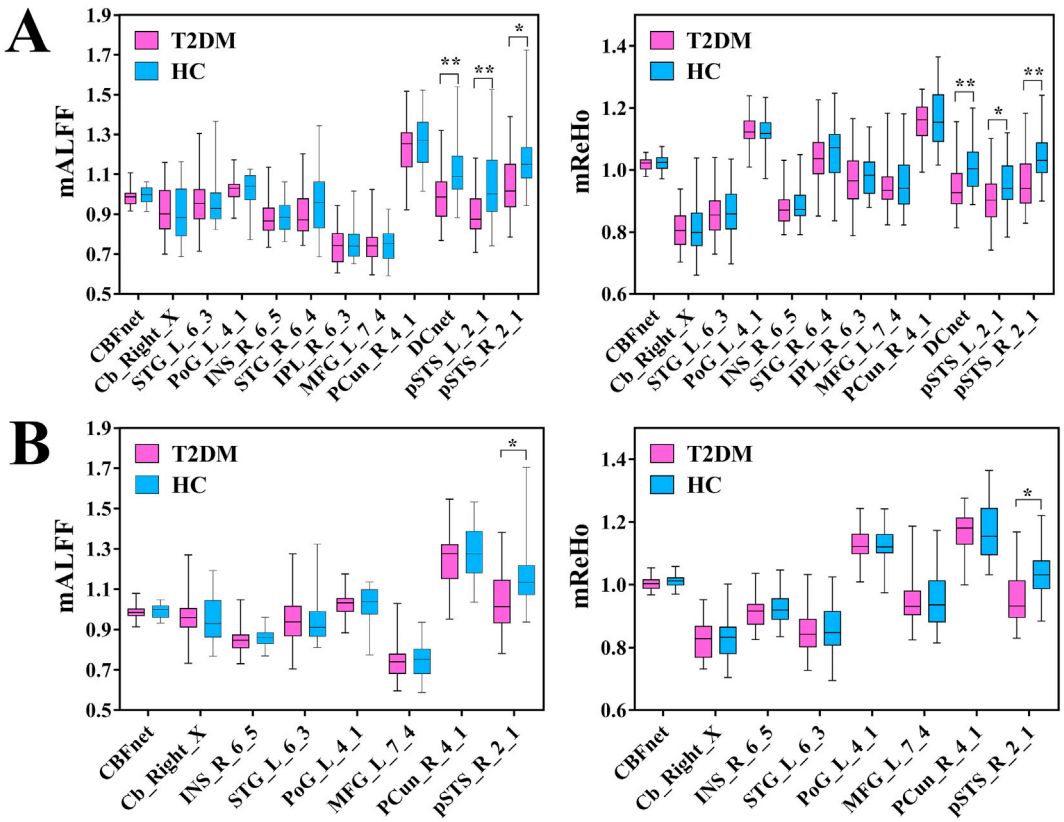

Fig. 3. Between-group comparison of mALFF and mReHo values in CBFnetwork and DCnetwork at region and network level. A., comparison in process regressed GMV; B., comparison in process without GMV regression. Abbreviation: CBFnet, CBFnetwork; DCnet, DCnetwork; Cb_Right_X, cerebellar lobule X, right; INS_R_6_5, dorsal granular insula, right; STG_L_6_3, superior temporal gyrus, part 3 (area TE), left; PoG_L_4_1, postcentral gyrus, part 1 (area 1/2/3 upper limb), left; MFG_L_7_4, middle frontal gyrus, part 4 (ventral area 9/46), left; PCun_R_4_1, precuneus, part 1 (medial area 7), right; STG_R_6_4, superior temporal gyrus, part 4 (caudal area 22), right; IPL_R_6_3, inferior parietal lobule, part 3 (rostrodorsal area 40), right; pSTS_L_2_1, posterior superior temporal sulcus, part 1 (rostroposterior superior temporal sulcus), left; pSTS_R_2_1, posterior superior temporal sulcus, part 1 (rostroposterior superior temporal sulcus), right. **, $P < 0.001$; *, $P < 0.05$.

group difference was found in CBF-mALFF coupling ($P_{FDR} = 0.854$) and CBF-mReHo coupling ($P_{FDR} = 0.886$). Besides, no significant intergroup difference was found in CBF/DC/mALFF/mReHo correlation matrix ($rDM = 0.05 \pm 0.26$, $rHC = 0.06 \pm 0.26$, $P = 0.462$) (Fig. 5A–B). For mReHonetwork, no significant intergroup difference was found in CBF/DC/mALFF/mReHo correlation matrix ($rDM = 0.05 \pm 0.26$, $rHC = 0.06 \pm 0.26$, $P = 0.322$) (Fig. 6A–B).

Regional coupling of CBF-DC, CBF-mALFF and CBF-mReHo in different networks were consistent with those of the whole network. As shown in Table 3 and Fig. 7, no difference of regional CBF-DC coupling was observed in CBFnetwork, while no difference of regional CBF-mALFF coupling and CBF-mReHo coupling was observed in DCnetwork. As shown in Fig. 8A, no significant difference of coupling of CBF-DC, CBF-mALFF and CBF-mReHo was found in mReHonetwork.

In the process without GMV regression, as illustrated in Table S3 and Figs. S3–4 in the Supplementary material, most results of network and regional coupling of CBF-DC, CBF-mALFF and CBF-mReHo were consistent with those with GMV regression except for the absence of significant intergroup differences in CBF-mALFF coupling ($P_{FDR} = 0.056$) and CBF-mReHo coupling ($P_{FDR} = 0.078$) of CBFnetwork. No significant intergroup difference was found in CBF/DC/mALFF/mReHo correlation matrix ($rDM = 0.07 \pm 0.31$, $rHC = 0.06 \pm 0.30$, $P = 0.097$). As shown in Fig. 6C–D and 8B, there was no intergroup difference in CBF/DC/mALFF/mReHo correlation matrix ($rDM = 0.07 \pm 0.31$, $rHC = 0.06 \pm 0.30$, $P = 0.934$) and coupling of CBF-DC, CBF-mALFF and CBF-mReHo in mReHonetwork.

3.7. Correlation results

After adjusted by FDR, HbA1c was negatively correlated with CBF-mALFF coupling and CBF-mReHo coupling in both PoG_L_4_1 and STG_R_6_4 as shown in Fig. 9. FBG was negatively correlated with CBF-mALFF coupling of CBFnetwork ($rDM = -0.412$, $P_{FDR} = 0.048$). Illness duration was positively correlated with the CBF-DC coupling in pSTS_L_2_1 ($rDM = -0.488$, $P_{FDR} = 0.019$). In terms of cognitive performance, NRT was negatively correlated with CBF-mALFF coupling and CBF-mReHo coupling in both CBFnetwork and MFG_L_7_4 (Fig. 10). NCR was negatively correlated with CBF-mALFF coupling in CBFnetwork ($rDM = -0.481$, $P_{FDR} = 0.036$). In addition, MMSE scores was positively correlated with CBF-mALFF coupling in Cb_Right_X ($rDM = -0.461$, $P_{FDR} = 0.046$). NCR was positively correlated with NRT in both T2DM ($r = 0.936$, $P_{FDR}<0.001$) group and HC group ($r = 0.967$, $P_{FDR}<0.001$). CBF value in CBFnetwork was negatively correlated with NRT ($rDM = -0.531$, $P_{FDR} = 0.022$) and NCR ($rDM = -0.506$, $P_{FDR} = 0.037$) respectively. mALFF in pSTS_L_2_1 was negatively correlated with MMSE score ($rDM = -0.323$, $P_{FDR} = 0.031$) (Fig. S5 in the Supplementary material).

In the process without GMV regression, HbA1c was negatively correlated with CBF-mALFF coupling ($rDM = -0.500$, $P_{FDR} = 0.012$) and CBF-mReHo coupling ($rDM = -0.507$, $P_{FDR} = 0.011$) in PoG_L_4_1 as shown in Fig. S6 in the Supplementary material. NRT was negatively correlated with CBF-mALFF coupling and CBF-mReHo coupling in both CBFnetwork and MFG_L_7_4 as shown in Fig. S7. NCR was negatively correlated with CBF-mALFF coupling and CBF-mReHo coupling in

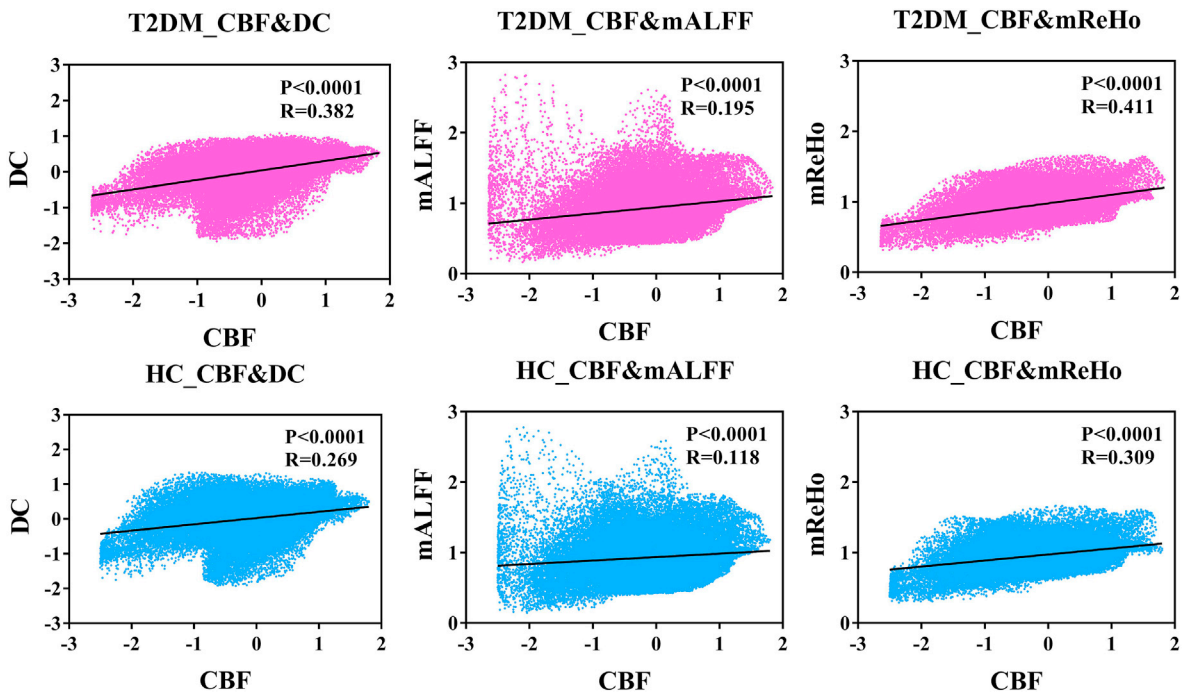

Fig. 4. CBF-DC, CBF-mALFF and CBF-mReHo coupling at the global level in HC and T2DM groups. Pink dot, T2DM group; light blue dot, HC group; &, coupling. Abbreviation: T2DM, type 2 diabetes mellitus; HC, healthy control; CBF, cerebral blood flow; DC, degree centrality; mALFF, mean amplitude of low-frequency fluctuation; mReHo, mean regional homogeneity.

CBFnetwork. No significant correlation was found between individual CBF, DC, mALFF, mReHo values and cognitive performance at region level and network level.

4. Discussion

NV decoupling plays a critical role in diabetes-related Alzheimer's disease. In the current study, we demonstrated the significant correlation between blood perfusion and neural activity at global level in HC and T2DM groups, as well as the significant disruption of blood supply-neural activity coupling in hubs and hub-based networks in T2DM without MCI patients. Most regions in the networks mainly located in DMN. More importantly, the coupling of CBF-DC, CBF-mALFF and CBF-mReHo increased with better cognitive performance in T2DM group, to some extent. Coupling of CBF-DC, CBF-mALFF and CBF-mReHo potentially played an important role in the organization of cognitive network in early T2DM.

4.1. Slight cognitive alteration and significantly mismatched CBF, DC alterations were detected in T2DM patients without MCI

T2DM is a significant risk factor for MCI and is associated with an increased incidence of dementia when co-existing with MCI, according to longitudinal studies of large T2DM cohort (Pal et al., 2018)' (Artero et al., 2008; Li et al., 2011; Morris et al., 2014; Ciudin et al., 2017). Before MCI, the general cognitive function in T2DM patients remains "normal" for a long period, while the complex pathological changes of T2DM keep undermining patient's cognitive function (Ma et al., 2015; Zilliox et al., 2016). Our study indicated that the subtle alterations in the cognitive subitems, perfusion, and neural activity can be detected in T2DM without MCI patients. This finding suggested that T2DM without MCI patients may be the optimal target population for preventive intervention. Previous studies have suggested different alteration patterns between cerebral perfusion, and neural activity in T2DM patients (Cui et al., 2017; Yang et al., 2016). Our results confirmed this hypothesis by showing significantly different distribution of CBF and DC metrics simultaneously measured in the same cohort.

4.2. Networks with hubs mainly located in DMN

DMN, mainly including the posterior cingulate cortex/precuneus, medial prefrontal cortex (mPFC), dorsal mPFC, temporoparietal junction, temporal lobe and posterior inferior parietal lobe, is regarded as the most important resting-state network system to be studied (Qi et al., 2017; Liu et al., 2019). Dysfunction of DMN was found before memory impairments in T2DM (Chen et al., 2016b). The alterations of DMN sub-networks were also different from each other between T2DM patients and HC subjects (Cui et al., 2015). In accordance with previous studies, we identified that the most regions in our CBFnetwork and DCnetwork located in DMN, indicating that DMN is the main network impaired in early T2DM patients.

Among those regions, bilateral temporal lobes were heavily involved. Besides, DCnetwork was even restricted to the superior temporal gyrus. Previous studies reported that T2DM patients exhibited decreased GMV in certain brain regions, including the superior and middle temporal gyri (Zhang et al., 2014). Taking GMV into consideration, more regions in temporal gyrus were found in our study indicating that bilateral temporal gyrus was impaired even without any GM atrophy in T2DM patients.

Cb_Right_X was another critical region that was involved in the CBFnetwork. In addition to regulating balance and eye movements, recent human and rodent studies have shown that cerebellar regions were related to cognitive function in different aspects, such as cognitive flexibility, spatial navigation, working memory and certain types of discrimination learning under aging and disease states (Shipman and Green, 2019; Liang and Carlson, 2019). In T2DM patients, decrease in anatomical connections, mReHo and CBF were reported in cerebellar regions (Dai et al., 2017; Peng et al., 2016; Fang et al., 2017). In accordance with previous studies, decreased coupling of CBF-mALFF and CBF-mReHo were also observed in the current study, adding evidence to the important role of the cerebellum in the cognitive process. In addition,

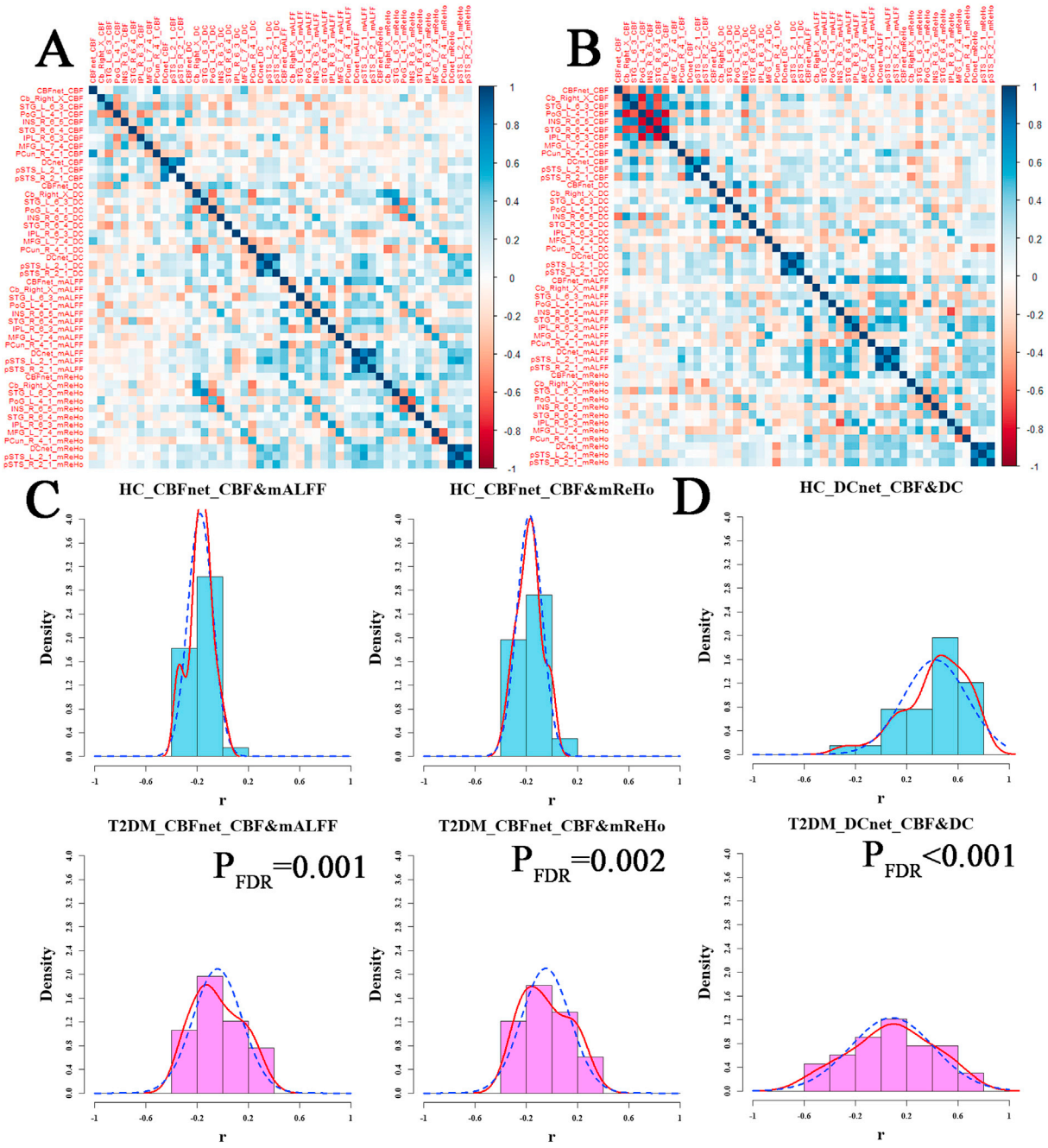

Fig. 5. Regional and networks cross-modality relationship. No significant intergroup difference in CBF/DC/mALFF/mReHo correlation matrix was found at network level between HC (A) and T2DM (B) (rHC = 0.06 ± 0.25, rDM = 0.05 ± 0.27, P = 0.63). Significantly increased CBF-mALFF and CBF-mReHo coupling were found in CBFnetwork (C), while significantly decreased CBF-DC coupling were found in DCnetwork (D). Histogram, probability distribution of altered coupling coefficients of CBF-DC, CBF-mALFF and CBF-mReHo across subjects, averaged across networks; Blue dashed line, corresponding normal distribution; Blue histogram, HC group; pink histogram, T2DM without MCI group; &, coupling between CBF and neural activity; red line, density curve. P_{FDR}, p value corrected by FDR.

CBF-mALFF coupling rather than individual CBF in Cb_Right_X was positively related with MMSE score indicated the potential value of CBF-mALFF coupling in exploring the mechanism of diabetic cognitive impairment.

4.3. Coupling of CBF-DC, CBF-mALFF and CBF-mReHo - potential biomarkers for diabetic cognitive impairment

It is out of our expectation that though CBF was significantly correlated with DC, mALFF, mReHo, no significant group difference was found at the global level. This may be the reason that most T2DM patient can maintain normal cognitive function for a long time, though decreased CBF and DC exist and some subitems of various cognitive dimensions are impaired gradually (Iadecola, 2017; Lecrux and Hamel, 2011). In terms of region and network level, CBFnetwork and DCnetwork were altered differently. In CBFnetwork, CBF-mALFF and CBF-mReHo coupling changed significantly between groups, while CBF-DC coupling changed significantly in DCnetwork. This trend may be because of the consistent changes between DC and mALFF, mReHo as shown in ours and previous studies (Cha et al., 2015; Zhu et al., 2018). DC, mALFF and mReHo reflect the activity characteristics of brain neurons from different aspects. In addition, these sensitive indicators were significantly correlated with

Table 3
Group differences of regional and network coupling of CBF-DC, CBF-mALFF and CBF-mReHo in the process regressed GMV.

CBF-cortical activity	T2DM group	HC group	P_{FDR}
CBFnet_CBF_DC	0.08(0.13)	0.03(0.12)	0.168
CBFnet_CBF_mALFF	−0.04(0.19)	−0.17(0.10)	0.001*
CBFnet_CBF_mReHo	−0.05(0.19)	−0.17(0.10)	0.002*
Cb_Right_X_CBF_DC	0.24(0.36)	0.35(0.34)	0.265
Cb_Right_X_CBF_mALFF	−0.65(0.22)	−0.44(0.27)	0.002*
Cb_Right_X_CBF_mReHo	0.44(0.26)	0.21(0.28)	0.002*
STG_L_6_3_CBF_DC	0.10(0.23)	0.18(0.23)	0.224
STG_L_6_3_CBF_mALFF	0.52(0.33)	0.76(0.17)	0.001*
STG_L_6_3_CBF_mReHo	0.52(0.32)	0.75(0.17)	0.001*
PoG_L_4_1_CBF_DC	0.01(0.26)	−0.12(0.21)	0.058
PoG_L_4_1_CBF_mALFF	−0.15(0.59)	−0.61 (0.17)	0.000**
PoG_L_4_1_CBF_mReHo	−0.18 (0.59)	−0.64(0.17)	0.000**
INS_R_6_5_CBF_DC	0.06(0.18)	0.14(0.20)	0.191
INS_R_6_5_CBF_mALFF	0.32(0.40)	0.71(0.12)	0.000**
INS_R_6_5_CBF_mReHo	0.27(0.43)	0.68(0.15)	0.000**
STG_R_6_4_CBF_DC	0.15(0.33)	−0.31(0.36)	0.059
STG_R_6_4_CBF_mALFF	−0.27(0.66)	−0.66(0.25)	0.004*
STG_R_6_4_CBF_mReHo	−0.34(0.67)	−0.73(0.24)	0.004*
IPL_R_6_3_CBF_DC	0.13(0.25)	0.17(0.25)	0.644
IPL_R_6_3_CBF_mALFF	0.53(0.46)	0.86(0.10)	0.000**
IPL_R_6_3_CBF_mReHo	0.50(0.47)	0.84(0.10)	0.000**
MFG_L_7_4_CBF_DC	0.08(0.25)	0.10(0.31)	0.854
MFG_L_7_4_CBF_mALFF	0.54(0.32)	0.78(0.14)	0.001*
MFG_L_7_4_CBF_mReHo	0.54(0.32)	0.79(0.13)	0.000**
PCun_R_4_1_CBF_DC	0.02(0.22)	−0.24(0.29)	0.612
PCun_R_4_1_CBF_mALFF	−0.21(0.43)	−0.41(0.35)	0.000**
PCun_R_4_1_CBF_mReHo	−0.03(0.42)	−0.42(0.34)	0.000**
DCnet_CBF_DC	0.09(0.32)	0.42(0.25)	0.000**
DCnet_CBF_mALFF	0.69(0.11)	0.68(0.11)	0.854
DCnet_CBF_mReHo	0.67(0.12)	0.67(0.09)	0.886
pSTS_L_2_1_CBF_DC	0.01(0.32)	0.31(0.36)	0.001*
pSTS_L_2_1_CBF_mALFF	0.60(0.30)	0.61(0.22)	0.905
pSTS_L_2_1_CBF_mReHo	0.56(0.30)	0.59(0.23)	0.854
pSTS_R_2_1_CBF_DC	0.12(0.39)	0.47(0.28)	0.000**
pSTS_R_2_1_CBF_mALFF	0.72(0.14)	0.72(0.14)	0.878
pSTS_R_2_1_CBF_mReHo	0.71(0.14)	0.71(0.11)	0.971

Data are presented as mean (SD); &, coupling; **, $P < 0.001$; *, $P < 0.05$.

cognitive performance and disease severity. Thus, it is very important to explore all these coupling indicators, rather than only CBF-DC coupling (Zhu et al., 2017; Sheng et al., 2018), to integrate the overall information.

Most CBF-mALFF coupling and CBF-mReHo coupling were negatively correlated with NRT which meant that the higher coupling coefficient, the shorter time to react to neutral card. However, there was negative correlation between CBF-mALFF coupling in CBFnetwork and NCR. As long as is concerned, this may be due to the positive correlation between NRT and NCR rather than negative intrinsic relationship between CBF-mALFF coupling and cognitive performance. To our surprise, the CBF-DC coupling of pSTS_L_2_1 was positively correlated with T2DM duration. The majority of T2DM patients were treated with insulin and metformin. As is reported, metformin can rapidly penetrate the blood–brain barrier to protect neurons through anti-inflammatory processes and improvement of brain energy metabolism so as to improve cognitive function (Lin et al., 2018; Foretz and Viollet, 2014). Considering the risk of peripheral hypoglycemia, the function of insulin is controversial. However, there were still series of studies hinted that low dose insulin can improve cognitive function (Freiherr et al., 2013; Craft et al., 2012). Our findings could therefore be attributed to the beneficial effect of the medications, but many other plausible explanations can be expected. For example, the lifestyle change and exercise.

4.4. Potential physiological meanings

DC is defined as the number of links that are strongly correlated to a given voxel or node for a binary graph and enables whole brain analysis at the voxel level, avoiding the bias caused by priori assumption (Zuo et al., 2012). It can quantify the importance of a node to the rest of the brain, and nodes with high DC are defined as hubs (Liu et al., 2018). Thus, decreased CBF-DC coupling in DCnetwork may reflect that though functional connectivity was disrupted in these regions, blood supply struggled to maintain the normal perfusion in order to compensate the impairment (Liang et al., 2013).

mALFF is defined as the total power within low frequency range (0.01 Hz–0.1 Hz) and is considered to be physiologically meaningful and reflective of spontaneous neural activity, while mReHo represent the consistency of BOLD signal fluctuations in a specific region reflecting near-neural activity arising at the same frequency. Considering no region with altered mALFF or mReHo was found in CBFnetwork, the decreased absolute value of CBF-mALFF coupling and CBF-mReHo coupling in CBFnetwork may indicate the incongruous between the requirement of oxygen and the blood supply.

Regional mALFF and mReHo decreased in DCnetwork in present study. Although some previous studies have demonstrated possible overlaps between findings from ALFF and functional connectivity analyses (Aiello et al., 2015; Sato et al., 2019), the neurobiological mechanisms linking the local ALFF and DC remain unknown. A hypothesis to explain this is that the hub regions are expected to present a greater variability in spontaneous activation. Regional decrease of DC may owe to the reduced mean neural activity intensity of simultaneous fluctuations with the other global voxels (Aiello et al., 2015; Buzsaki and Draguhn, 2004). However, mALFF and mReHo are potentially proxies for local spontaneous neural activity, whereas DC indicates the relationship between the local activity and the global network dynamics. In accordance with most previous studies, most regions with altered DC, mALFF and mReHo did not match with each other using the voxel-wise analysis in present study (Cha et al., 2015; Wang et al., 2017; Tang et al., 2019). Since different functional networks, such as DMN, dorsal attention network, ventral attention network, executive control network, are activated under different activation states. The neural activation of each voxel in altered DC regions was inhomogeneous. This may be why the regions with altered mReHo values did not locate at the similar region with altered DC after voxel-wise analysis in the present study. Further study is needed to rule out the possibility of artifacts induced by other physiological signals such as cardiac or vascular systems. Besides, more neurobiology study is also needed to.

Many previous studies have reported that people with T2DM are susceptible to cerebrovascular diseases, especially in China (Zhang et al., 2018; Yang et al., 2013). Though no significant different BMI, blood pressure, triglycerides, total cholesterol, HDL or LDL was found between groups, the decreased CBF in Cb_Right_X, INS_R_6_5, STG_L_6_3, MFG_L_7_4, IPL_R_6_3 and decreased absolute coupling of CBF-DC, CBF-mALFF and CBF-mReHo may be the result of the cerebrovascular diseases, such as cerebral atherosclerosis, which can narrow the vessel diameter, decrease the vasoreactivity, yielding a decline of cerebral perfusion (Han et al., 2019) and gradually disorganize functional connectivity (Gianaros et al., 2009). Cerebrovascular diseases, especially cerebral small vessel disease (CSVD), are characterized by its insidious onset and slow progression (Wardlaw et al., 2013). However, once it eventually leads to serious consequences, such as cognitive decline, mental disorders and constipation, it may be too late to be treated. Thus, it is very important to evaluate the CSVD by exploring vascular reactivity through functional MRI in T2DM population in the future (McKetton et al., 2019). The increased CBF in other regions may compensate to those decreased perfusion (Cui et al., 2017).

Previous studies showed that significantly decreased GMV was found even in T2DM patients without MCI (Zhang et al., 2014; Callisaya et al., 2019). Though no significantly altered GMV was observed at global and voxel level in the current study, more altered regions and more correlations between image measures and cognitive performance were found in the process with GMV regression. Many previous studies showed that specific cerebral function relied on the neural structure of certain cortices, which were mainly evaluated by GMV (Sherrill et al., 2018; Wagshul et al., 2019; Gilaie-Dotan et al., 2012). In addition,

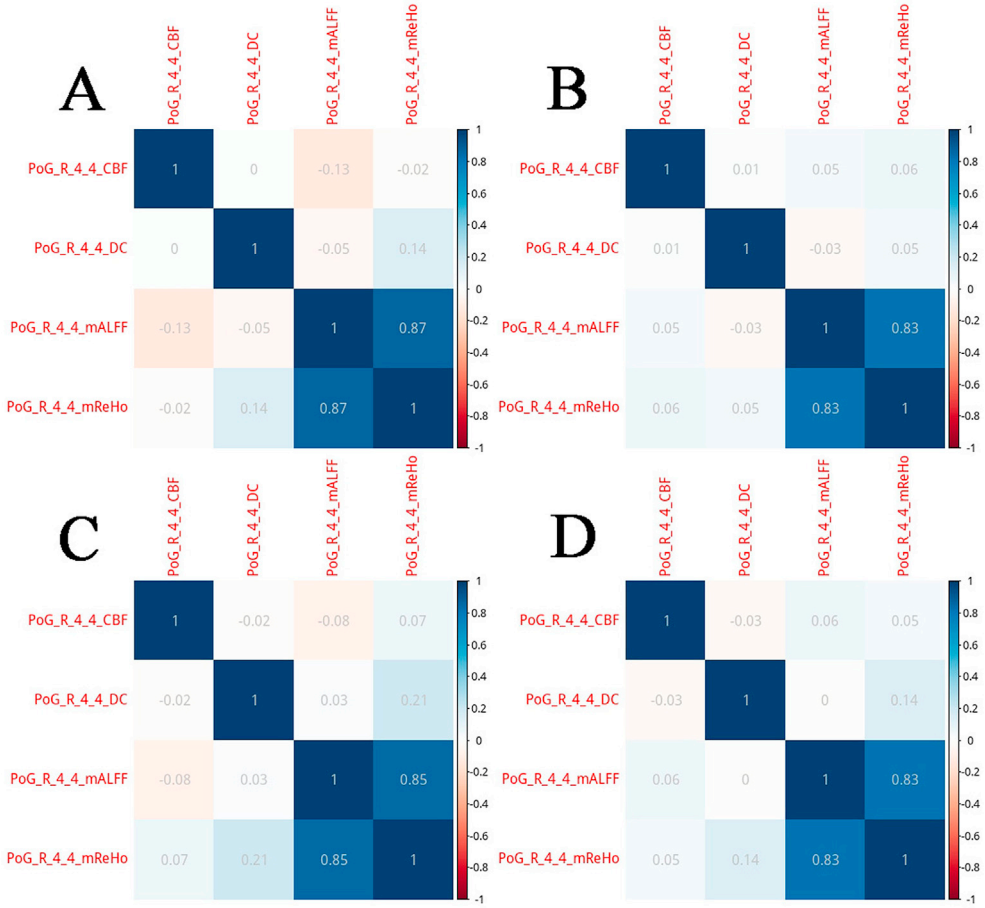

Fig. 6. mReHonetwork cross-modality relationship in HC and T2DM groups. In the process regressed GMV, no significant difference in CBF/DC/mALFF/mReHo correlation matrix was found at network level between HC (A) and T2DM (B) (rHC = 0.06 ± 0.25, rDM = 0.05 ± 0.27, P = 0.322). The same went for processes without GMV regression (rHC = 0.06 ± 0.25, rDM = 0.05 ± 0.27, P = 0.934).

inter-individual variability in a wide range of basic and higher cognitive functions, including perception, motor control, memory, and aspects of consciousness, were closely related with the local structure of GM as assessed by voxel-based morphometry (Doucet et al., 2019; Kong et al., 2019; Kanai and Rees, 2011). Thus, it is very important to take GMV effect into consideration when dealing with studies on NV coupling. In the current study, we took GMV as a covariate and regressed the signal of WM, GM and CSF, and 24-motion vectors managing to reach as close to the ground truth as possible. However, considering the contradictory views for regression (Saad et al., 2012; Fox et al., 2009), more research needs to be done to verify the necessity of GMV regression. In the process without GMV regression, CBF-mALFFor CBF-mReHo coupling rather than individual CBF, DC, mALFF, mReHo values were significantly correlated with cognitive performance. Since NV coupling plays a pivotal role in maintaining the normal brain function by providing the sufficient blood. This phenomenon may indicate that coupling of CBF-DC, CBF-mALFF and CBF-mReHo are more sensitive to cognitive impairment and closer to the true cognitive functional mechanism.

4.5. Limitations and future directions

Our study is limited by its relatively small sample size (n = 66) and cross-sectional design. In the current study, BOLD derived indicators, i.e. DC, mALFF, mReHo, were taken to reflect different characteristics of neural activity. These measurements were common in clinical practice and easy to implement, contributing to subsequent long-term observation. However, these indicators were indirect measures and may be affected by several physiological factors such as blood pressure, changes in the vascular bed, astrocytes and metabolites. Therefore, our results should be comprehended cautiously. In addition, task-fMRI or other measures that can reflect the neuronal responsiveness more directly should be used to verify our results in the future (Jamadar et al., 2019; Danjou et al., 2019). According to our results, coupling of CBF-DC, CBF-mALFF and CBF-mReHo of sub-regions in cerebellum may play important roles in the cognitive alterations of early T2DM. Thus, further studies are needed to investigate the functional role of these regions for the organization of advanced cognitive process.

5. Conclusion

Cognitive, perfusion, neural activity and NV coupling alterations were detectable in T2DM patients without MCI. Early and subtle cognitive alterations, underpinned by decreased perfusion and neural activity, may represent an early harmful effect of T2DM to both vascular and neuronal systems. Decrease in the absolute coupling of CBF-DC, CBF-mALFF and CBF-mReHo in hub-based networks indicated NV decoupling, while the significant correlation between coupling of CBF-DC, CBF-mALFF or CBF-mReHo and cognitive performance, disease severity, may hint that coupling of CBF-DC, CBF-mALFF and CBF-mReHo are more sensitive to the cognitive impairment in early T2DM. Our results contribute to a better understanding of the mechanism for the cognitive impairment in T2DM and its neuroimaging biomarkers.

Funding

This work was supported by the National Natural Science Foundation

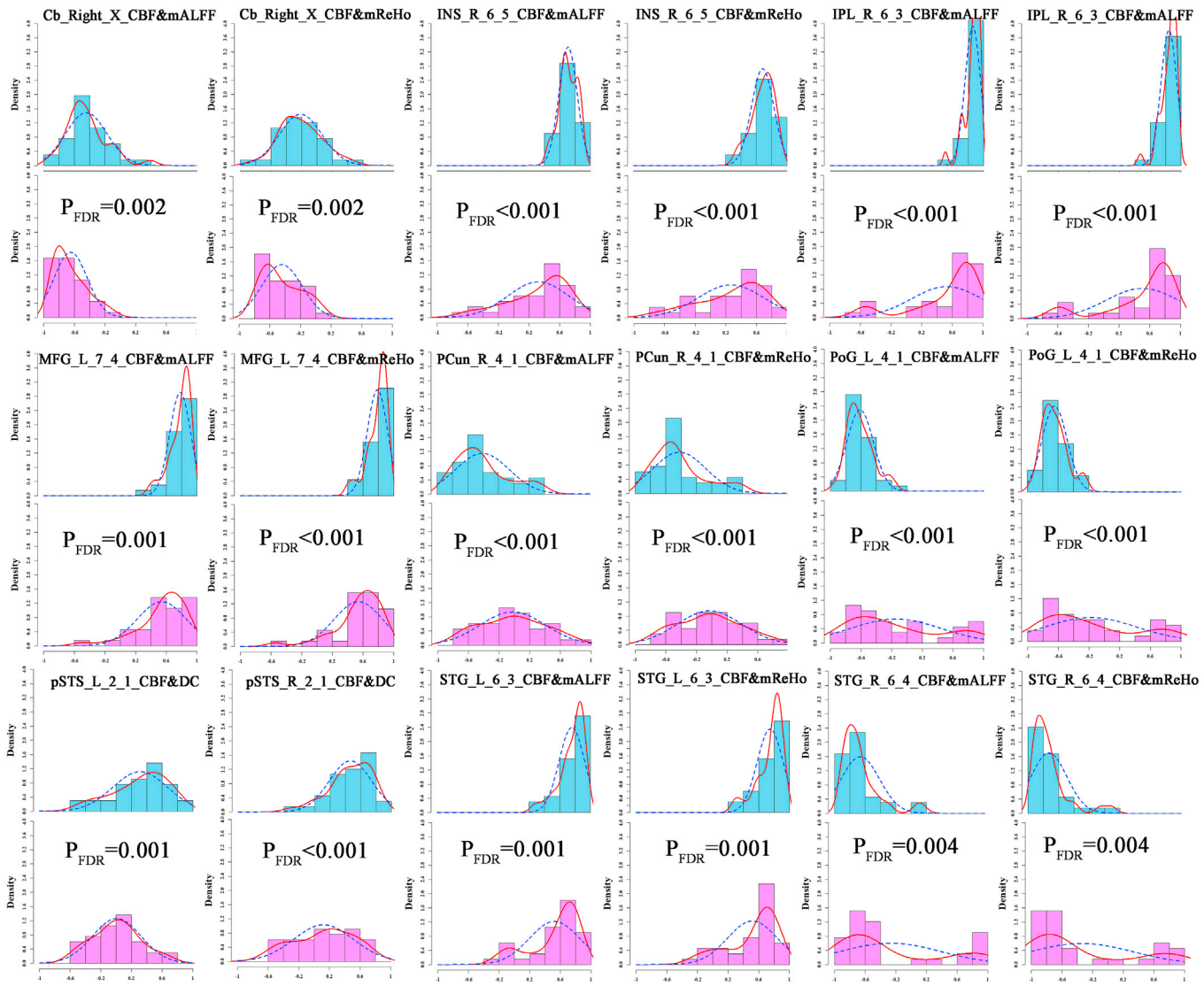

Fig. 7. Significantly altered regional CBF-neural activity coupling coefficient in HC and T2DM groups. Histogram, probability distribution of altered coupling coefficients of CBF-DC, CBF-mALFF and CBF-mReHo across subjects, averaged across networks; Blue dashed line, corresponding normal distribution; Blue histogram, HC group; pink histogram, T2DM without MCI group; &, coupling between CBF and neural activity; red line, density curve. P_{FDR}, p value corrected by FDR.

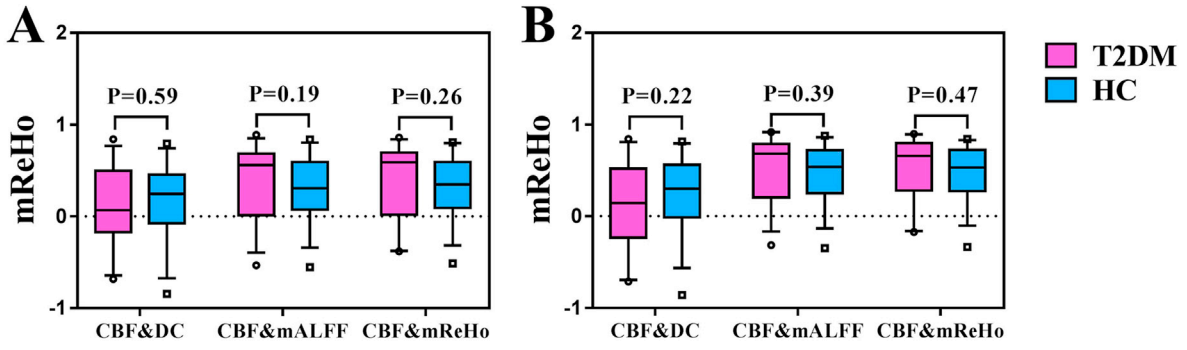

Fig. 8. Comparison of CBF-DC, CBF-mALFF and CBF-mReHo coupling in mReHonetwork. Intergroup comparisons were explored in process with (A) or without (B) GMV regression. No significant group difference was found in both processes.

of China [grant numbers 81471636, 81771815, 81801676]; the National Key Research and Development Program of China [grant number 2016YFC0107105]; the Shaanxi International Science and Technology Cooperation and Exchange Program [grant number 2015KW-039]; the Innovation and Development Foundation of Tangdu Hospital [grant number 2014JSYJ002, 2015JSYJ003, 2016JCYJ002], the Talent Foundation of Tangdu Hospital to Wen Wang and the Seeding Talent Foundation of Tangdu Hospital to Yu Ying.

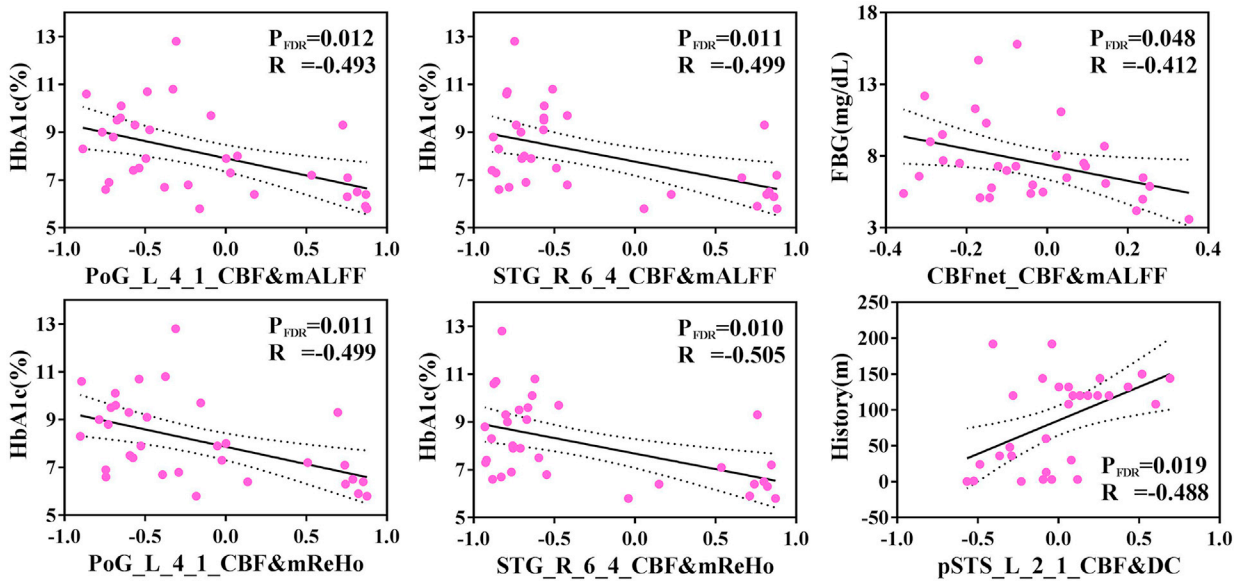

Fig. 9. Significant correlations between CBF-activation coupling and disease severity in CBFnetwork and DCnetwork in T2DM patients. HbA1c, glycosylated hemoglobin A1c; FBG, Fasting blood glucose; m, month; PoG_L_4_1, postcentral gyrus, part 1 (area 1/2/3 upper limb), left; STG_R_6_4, superior temporal gyrus, part 4 (caudal area 22), right; CBFnet, CBFnetwork; pSTS_L_2_1, posterior superior temporal sulcus, part 1 (rostroposterior superior temporal sulcus), left; P_{FDR}, p value corrected by FDR; R, correlation coefficient. &, coupling.

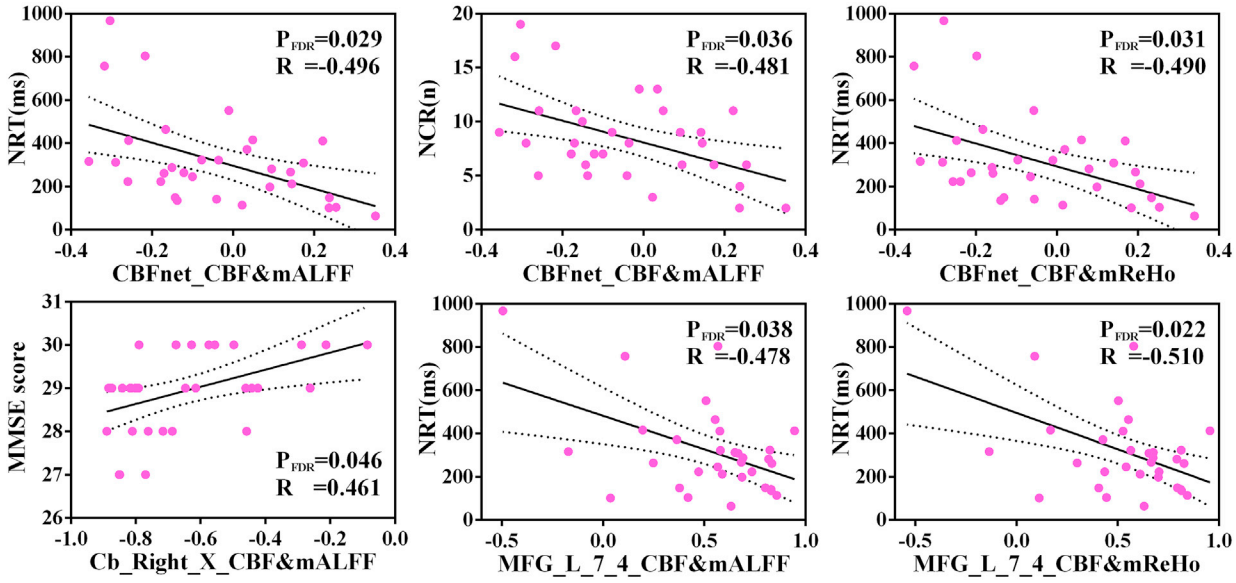

Fig. 10. Significant correlations between CBF-activation coupling and cognitive performance in CBFnetwork and DCnetwork in T2DM patients. NRT, neutral reaction time; NCR, neutral correct response; MMSE, mini-mental state examination; CBFnet, CBFnetwork; Cb_Right_X, cerebellar lobule X, right; MFG_L_7_4, middle frontal gyrus, part 4 (ventral area 9/46), left; P_{FDR}, p value corrected by FDR; R, correlation coefficient. &, coupling.

Author contributions

Wen Wang and Guang-Bin Cui were the guarantors of this work and, as such, had full access to all the data in the study and take responsibility for the integrity of the data and the accuracy of the data analysis. Ying Yu, Lin-Feng Yan, Qian Sun and Bo Hu contributed equally to this article.

Study concept and design: Ying Yu, Bo Hu, Guang-Bin Cui and Wen Wang.

Acquisition, analysis, or interpretation of data: Ying Yu, Lin-Feng Yan, Qian Sun, Bo Hu, Jin Zhang, Yang Yang, Yu-Jie Dai, Wu-Xun Cui, Si-Jie Xiu, Yu-Chuan Hu, Chun-Ni Heng, Qing-Quan Liu, Jun-Feng Hou.

Drafting of the manuscript: Ying Yu, Bo Hu and Wen Wang.

Critical revision of the manuscript for important intellectual content: Ying Yu, Lin-Feng Yan, Qian Sun, Bo Hu, Jin Zhang, Yang Yang, Yu-Jie Dai, Wu-Xun Cui, Si-Jie Xiu, Yu-Chuan Hu, Chun-Ni Heng, Qing-Quan Liu, Jun-Feng Hou, Yu-Yun Pan, Liang-Hao Zhai, Teng-Hui Han, Wen Wang, Guang-Bin Cui.

Statistical analysis: Yu-Yun Pan, Liang-Hao Zhai, Teng-Hui Han.

Obtained funding: Ying Yu, Wen Wang, Guang-Bin Cui.

Administrative, technical, or material support: Wu-Xun Cui, Si-Jie Xiu, Yu-Chuan Hu, Chun-Ni Heng, Qing-Quan Liu, Jun-Feng Hou, Wen Wang and Guang-Bin Cui.

Study supervision: Wen Wang and Guang-Bin Cui.

Declaration of conflicting interests

The author(s) declared no potential conflicts of interest with respect to the research, authorship, and/or publication of this article.

Acknowledgments

The authors want to thank the clinical and the nursing team of the Endocrinology Department in Tangdu Hospital for their cooperation with working on patients' recruiting. The authors are grateful to Prof. Lin Shi for critical help with multiple comparison correction. Our gratitude goes to Prof. Chun-Shui Yu, Drs. Wen Qin, Feng Liu from the Department of Radiology, Tianjin Medical University General Hospital and Meng Liang from the School of Medical Imaging, Tianjin Medical University for their selfishless help to our group. Our gratitude also goes to the team of Shen Zhen Sinorad Medical Electronics Co., Ltd and Mr. Xiao-Cheng Wei (MR research, GE Healthcare China) for their continuous technique support.

Appendix A. Supplementary data

Supplementary data to this article can be found online at https://doi.org/10.1016/j.neuroimage.2019.06.058.

References

Aiello, M., Salvatore, E., Cachia, A., et al., 2015. Relationship between simultaneously acquired resting-state regional cerebral glucose metabolism and functional MRI: a PET/MR hybrid scanner study. Neuroimage 113, 111–121.
Alsop, D.C., Detre, J.A., Golay, X., et al., 2015. Recommended implementation of arterial spin-labeled perfusion MRI for clinical applications: a consensus of the ISMRM perfusion study group and the European consortium for ASL in dementia. Magn. Reson. Med. 73, 102–116.
American Diabetes, A., 2014. Diagnosis and classification of diabetes mellitus. Diabetes Care 37 (Suppl. 1), S81–S90.
Artero, S., Ancelin, M.-L., Portet, F., et al., 2008. Risk profiles for mild cognitive impairment and progression to dementia are gender specific. Journal of Neurology, Neurosurgery & Psychiatry 79, 979–984.
Bae, J.S., Kim, O.K., Kim, J.M., 2011. Altered nerve excitability in subclinical/early diabetic neuropathy: evidence for early neurovascular process in diabetes mellitus? Diabetes Res. Clin. Pract. 91, 183–189.
Beauquis, J., Homo-Delarche, F., Giroix, M.H., et al., 2010. Hippocampal neurovascular and hypothalamic-pituitary-adrenal axis alterations in spontaneously type 2 diabetic GK rats. Exp. Neurol. 222, 125–134.
Buzsaki, G., Draguhn, A., 2004. Neuronal oscillations in cortical networks. Science 304, 1926–1929.
Callisaya, M.L., Beare, R., Moran, C., Phan, T., Wang, W., Srikanth, V.K., 2019. Type 2 diabetes mellitus, brain atrophy and cognitive decline in older people: a longitudinal study. Diabetologia 62, 448–458.
Cerasuolo, J., Izzo, A., 2017. Persistent impairment in working memory following severe hyperglycemia in newly diagnosed type 2 diabetes. Endocrinology, diabetes & metabolism case reports 2017.
Cha, J., Hwang, J.M., Jo, H.J., Seo, S.W., Na, D.L., Lee, J.M., 2015. Assessment of functional characteristics of amnestic mild cognitive impairment and Alzheimer's disease using various methods of resting-state FMRI analysis. BioMed Res. Int. 2015, 907464.
Chen, G., Chen, G., Xie, C., et al., 2012. A method to determine the necessity for global signal regression in resting-state fMRI studies. Magn. Reson. Med. 68, 1828–1835.
Chen, J., Shu, H., Wang, Z., et al., 2016. Convergent and divergent intranetwork and internetwork connectivity patterns in patients with remitted late-life depression and amnestic mild cognitive impairment. Cortex; a journal devoted to the study of the nervous system and behavior 83, 194–211.
Chen, Y., Liu, Z., Wang, A., et al., 2016. Dysfunctional organization of default mode network before memory impairments in type 2 diabetes. Psychoneuroendocrinology 74, 141–148.
Ciudin, A., Espinosa, A., Simo-Servat, O., et al., 2017. Type 2 diabetes is an independent risk factor for dementia conversion in patients with mild cognitive impairment. J. Diabetes Complicat. 31, 1272–1274.
Craft, S., Baker, L.D., Montine, T.J., et al., 2012. Intranasal insulin therapy for Alzheimer disease and amnestic mild cognitive impairment: a pilot clinical trial. Arch. Neurol. 69, 29–38.
Cui, Y., Jiao, Y., Chen, Y.C., et al., 2014. Altered spontaneous brain activity in type 2 diabetes: a resting-state functional MRI study. Diabetes 63, 749–760.
Cui, Y., Jiao, Y., Chen, H.J., et al., 2015. Aberrant functional connectivity of default-mode network in type 2 diabetes patients. Eur. Radiol. 25, 3238–3246.
Cui, Y., Li, S.F., Gu, H., et al., 2016. Disrupted brain connectivity patterns in patients with type 2 diabetes. AJNR Am. J. Neuroradiol. 37, 2115–2122.
Cui, Y., Liang, X., Gu, H., et al., 2017. Cerebral perfusion alterations in type 2 diabetes and its relation to insulin resistance and cognitive dysfunction. Brain Imag. Behav. 11, 1248–1257.
Dai, W., Duan, W., Alfaro, F.J., Gavrieli, A., Kourtelidis, F., Novak, V., 2017. The resting perfusion pattern associates with functional decline in type 2 diabetes. Neurobiol. Aging 60, 192–202.
Danjou, P., Viardot, G., Maurice, D., et al., 2019. Electrophysiological assessment methodology of sensory processing dysfunction in schizophrenia and dementia of the Alzheimer type. Neurosci. Biobehav. Rev. 97, 70–84.
Del Zoppo, G.J., 2013. Toward the neurovascular unit. A journey in clinical translation: 2012 Thomas Willis Lecture. Stroke 44, 263–269.
Doucet, G.E., Moser, D.A., Rodrigue, A., Bassett, D.S., Glahn, D.C., Frangou, S., 2019. Person-based brain morphometric similarity is heritable and correlates with biological features. Cerebr. Cortex 29, 852–862.
Duarte, J.V., Pereira, J.M., Quendera, B., et al., 2015. Early disrupted neurovascular coupling and changed event level hemodynamic response function in type 2 diabetes: an fMRI study. J. Cereb. Blood Flow Metab. 35, 1671–1680.
Fan, L., Li, H., Zhuo, J., et al., 2016. The human brainnetome Atlas: a new brain Atlas based on connectional Architecture. Cerebr. Cortex 26, 3508–3526.
Fang, P., An, J., Tan, X., et al., 2017. Changes in the cerebellar and cerebro-cerebellar circuit in type 2 diabetes. Brain Res. Bull. 130, 95–100.
Foretz, M., Viollet, B., 2014. [New promises for metformin: advances in the understanding of its mechanisms of action]. M-S (Med. Sci.): Méd. Sci. 30, 82–92.
Fox, M.D., Zhang, D., Snyder, A.Z., Raichle, M.E., 2009. The global signal and observed anticorrelated resting state brain networks. J. Neurophysiol. 101, 3270–3283.
Freiherr, J., Hallschmid, M., Frey 2nd, W.H., et al., 2013. Intranasal insulin as a treatment for Alzheimer's disease: a review of basic research and clinical evidence. CNS Drugs 27, 505–514.
Gianaros, P.J., Hariri, A.R., Sheu, L.K., Muldoon, M.F., Sutton-Tyrrell, K., Manuck, S.B., 2009. Preclinical atherosclerosis covaries with individual differences in reactivity and functional connectivity of the amygdala. Biol. Psychiatry 65, 943–950.
Gibas, K.J., 2017. The starving brain: overfed meets undernourished in the pathology of mild cognitive impairment (MCI) and Alzheimer's disease (AD). Neurochem. Int. 110, 57–68.
Gilaie-Dotan, S., Harel, A., Bentin, S., Kanai, R., Rees, G., 2012. Neuroanatomical correlates of visual car expertise. Neuroimage 62, 147–153.
Han, H., Zhang, R., Liu, G., et al., 2019. Reduction of cerebral blood flow in community-based adults with subclinical cerebrovascular atherosclerosis: a 3.0T magnetic resonance imaging study. Neuroimage 188, 302–308.
Hu, B., Yan, L.F., Sun, Q., et al., 2019. Disturbed neurovascular coupling in type 2 diabetes mellitus patients: evidence from a comprehensive fMRI analysis. NeuroImage Clin. 22, 101802.
Iadecola, C., 2017. The neurovascular unit coming of age: a journey through neurovascular coupling in health and disease. Neuron 96, 17–42.
Jamadar, S.D., Ward, P.G., Li, S., et al., 2019. Simultaneous task-based BOLD-fMRI and [18-F] FDG functional PET for measurement of neuronal metabolism in the human visual cortex. Neuroimage 189, 258–266.
Jansen, J.F., van Bussel, F.C., van de Haar, H.J., et al., 2016. Cerebral blood flow, blood supply, and cognition in Type 2 Diabetes Mellitus. Sci. Rep. 6, 10.
Kanai, R., Rees, G., 2011. The structural basis of inter-individual differences in human behaviour and cognition. Nat. Rev. Neurosci. 12, 231–242.
Khalili-Mahani, N., van Osch, M.J., de Rooij, M., et al., 2014. Spatial heterogeneity of the relation between resting-state connectivity and blood flow: an important consideration for pharmacological studies. Hum. Brain Mapp. 35, 929–942.
Kong, F., Yang, K., Sajjad, S., Yan, W., Li, X., Zhao, J., 2019. Neural correlates of social well-being: gray matter density in the orbitofrontal cortex predicts social well-being in emerging adulthood. Soc. Cogn. Affect. Neurosci. 14, 319–327.
Last, D., Alsop, D.C., Abduljalil, A.M., et al., 2007. Global and regional effects of type 2 diabetes on brain tissue volumes and cerebral vasoreactivity. Diabetes Care 30, 1193–1199.
Lecrux, C., Hamel, E., 2011. The neurovascular unit in brain function and disease. Acta Physiol. 203, 47–59.
Li, J., Wang, Y.J., Zhang, M., et al., 2011. Vascular risk factors promote conversion from mild cognitive impairment to Alzheimer disease. Neurology 76, 1485–1491.
Li, H., Li, L., Shao, Y., et al., 2016. Abnormal intrinsic functional hubs in severe male obstructive sleep Apnea: evidence from a voxel-wise degree centrality analysis. PLoS One 11, e0164031.
Li, P., Ding, D., Ma, X.Y., et al., 2018. Altered intrinsic brain activity and memory performance improvement in patients with end-stage renal disease during a single dialysis session. Brain Imag. Behav. 12, 1640–1649.
Li, M., Yan, J., Li, S., et al., 2018. Altered gray matter volume in primary insomnia patients: a DARTEL-VBM study. Brain Imag. Behav. 12, 1759–1767.
Liang, K.J., Carlson, E.S., 2019. Resistance, vulnerability and resilience: a review of the cognitive cerebellum in aging and neurodegenerative diseases. Neurobiol. Learn. Mem. https://doi.org/10.1016/j.nlm.2019.01.004.
Liang, X., Zou, Q., He, Y., Yang, Y., 2013. Coupling of functional connectivity and regional cerebral blood flow reveals a physiological basis for network hubs of the human brain. Proc. Natl. Acad. Sci. U. S. A. 110, 1929–1934.
Liang, X., Connelly, A., Calamante, F., 2014. Graph analysis of resting-state ASL perfusion MRI data: nonlinear correlations among CBF and network metrics. Neuroimage 87, 265–275.
Lin, Y., Wang, K., Ma, C., et al., 2018. Evaluation of metformin on cognitive improvement in patients with non-dementia vascular cognitive impairment and abnormal glucose metabolism. Front. Aging Neurosci. 10, 227.
Liska, A., Galbusera, A., Schwarz, A.J., Gozzi, A., 2015. Functional connectivity hubs of the mouse brain. Neuroimage 115, 281–291.
Liu, D., Duan, S., Zhou, C., et al., 2018. Altered brain functional hubs and connectivity in type 2 diabetes mellitus patients: a resting-state fMRI study. Front. Aging Neurosci. 10, 55.

Liu, H., Liu, J., Peng, L., et al., 2019. Changes in default mode network connectivity in different glucose metabolism status and diabetes duration. NeuroImage Clin. 21, 101629.
Ma, F., Wu, T., Miao, R., Xiao, Y.Y., Zhang, W., Huang, G., 2015. Conversion of mild cognitive impairment to dementia among subjects with diabetes: a population-based study of incidence and risk factors with five years of follow-up. J. Alzheimer's Dis. 43, 1441–1449.
McKetton, L., Venkatraghavan, L., Rosen, C., et al., 2019. Improved white matter cerebrovascular reactivity after revascularization in patients with steno-occlusive disease. AJNR Am. J. Neuroradiol. 40, 45–50.
Mogi, M., Horiuchi, M., 2011. Neurovascular coupling in cognitive impairment associated with diabetes mellitus. Circ. J. : Offic J. Jpn Circ. Soc. 75, 1042–1048.
Morris, J.K., Vidoni, E.D., Honea, R.A., Burns, J.M., Alzheimer's Disease Neuroimaging, I., 2014. Impaired glycemia increases disease progression in mild cognitive impairment. Neurobiol. Aging 35, 585–589.
Muoio, V., Persson, P.B., Sendeski, M.M., 2014. The neurovascular unit - concept review. Acta Physiol. 210, 790–798.
Nelson, A.R., Sweeney, M.D., Sagare, A.P., Zlokovic, B.V., 2016. Neurovascular dysfunction and neurodegeneration in dementia and Alzheimer's disease. Biochim. Biophys. Acta 1862, 887–900.
Pal, K., Mukadam, N., Petersen, I., et al., 2018. Mild cognitive impairment and progression to dementia in people with diabetes, prediabetes and metabolic syndrome: a systematic review and meta-analysis. Soc. Psychiatry Psychiatr. Epidemiol. 53, 1149–1160.
Peng, J., Qu, H., Peng, J., et al., 2016. Abnormal spontaneous brain activity in type 2 diabetes with and without microangiopathy revealed by regional homogeneity. Eur. J. Radiol. 85, 607–615.
Qi, D., Wang, A., Chen, Y., et al., 2017. Default mode network connectivity and related white matter disruption in type 2 diabetes mellitus patients concurrent with amnestic mild cognitive impairment. Curr. Alzheimer Res. 14, 1238–1246.
Roberts, R.O., Knopman, D.S., Geda, Y.E., et al., 2014. Association of diabetes with amnestic and nonamnestic mild cognitive impairment. Alzheimer's Dementia 10, 18–26.
Saad, Z.S., Gotts, S.J., Murphy, K., et al., 2012. Trouble at rest: how correlation patterns and group differences become distorted after global signal regression. Brain Connect. 2, 25–32.
Sato, J.R., Biazoli Jr., C.E., Moura, L.M., et al., 2019. Association between Fractional Amplitude of Low-Frequency Spontaneous Fluctuation and Degree Centrality in Children and Adolescents. *Brain Connectivity*.
Shekhar, S., Wang, S., Mims, P.N., et al., 2017. Impaired cerebral Autoregulation-A common neurovascular pathway in diabetes may play a critical role in diabetes-related Alzheimer's disease. Curr. Res. Diabetes Obes. J. 2.
Shen, Y., Yao, J., Jiang, X., et al., 2015. Sub-hubs of baseline functional brain networks are related to early improvement following two-week pharmacological therapy for major depressive disorder. Hum. Brain Mapp. 36, 2915–2927.
Sheng, J., Shen, Y., Qin, Y., et al., 2018. Spatiotemporal, metabolic, and therapeutic characterization of altered functional connectivity in major depressive disorder. Hum. Brain Mapp. 39, 1957–1971.
Sherrill, K.R., Chrastil, E.R., Aselcioglu, I., Hasselmo, M.E., Stern, C.E., 2018. Structural differences in hippocampal and entorhinal gray matter volume support individual differences in first person navigational Ability. Neuroscience 380, 123–131.
Shipman, M.L., Green, J.T., 2019. Cerebellum and cognition: does the rodent cerebellum participate in cognitive functions? Neurobiol. Learn. Mem. https://doi.org/10.1016/j.nlm.2019.02.006.
Sun, Q., Chen, G.Q., Wang, X.B., et al., 2018. Alterations of white matter integrity and hippocampal functional connectivity in type 2 diabetes without mild cognitive impairment. Front. Neuroanat. 12, 21.
Tang, Y., Zhou, Q., Chang, M., et al., 2019. Altered Functional Connectivity and Low-Frequency Signal Fluctuations in Early Psychosis and Genetic High Risk. Schizophrenia research.
van Osch, M.J., Teeuwisse, W.M., Chen, Z., Suzuki, Y., Helle, M., Schmid, S., 2018. Advances in arterial spin labelling MRI methods for measuring perfusion and collateral flow. J. Cereb. Blood Flow Metab. 38, 1461–1480.
Wagshul, M.E., Lucas, M., Ye, K., Izzetoglu, M., Holtzer, R., 2019. Multi-modal neuroimaging of dual-task walking: structural MRI and fNIRS analysis reveals prefrontal grey matter volume moderation of brain activation in older adults. Neuroimage 189, 745–754.
Wang, J.B., Zheng, L.J., Cao, Q.J., et al., 2017. Inconsistency in abnormal brain activity across cohorts of ADHD-200 in children with attention deficit hyperactivity disorder. Front. Neurosci. 11, 320.
Wardlaw, J.M., Smith, C., Dichgans, M., 2013. Mechanisms of sporadic cerebral small vessel disease: insights from neuroimaging. Lancet Neurol. 12, 483–497.
Xie, C., Bai, F., Yuan, B., et al., 2015. Joint effects of gray matter atrophy and altered functional connectivity on cognitive deficits in amnestic mild cognitive impairment patients. Psychol. Med. 45, 1799–1810.
Xu, W., Caracciolo, B., Wang, H.X., et al., 2010. Accelerated progression from mild cognitive impairment to dementia in people with diabetes. Diabetes 59, 2928–2935.
Yan, C.G., Wang, X.D., Zuo, X.N., Zang, Y.F., 2016. DPABI: data processing & analysis for (Resting-State) brain imaging. Neuroinformatics 14, 339–351.
Yang, G., Wang, Y., Zeng, Y., et al., 2013. Rapid health transition in China, 1990-2010: findings from the global burden of disease study 2010. Lancet 381, 1987–2015.
Yang, S.Q., Xu, Z.P., Xiong, Y., et al., 2016. Altered intranetwork and internetwork functional connectivity in type 2 diabetes mellitus with and without cognitive impairment. Sci. Rep. 6, 32980.
Yang, Q., Zhou, L., Liu, C., et al., 2018. Brain iron deposition in type 2 diabetes mellitus with and without mild cognitive impairment-an in vivo susceptibility mapping study. Brain Imag. Behav. 12, 1479–1487.
Yuan, M., Zhu, H., Qiu, C., et al., 2016. Group cognitive behavioral therapy modulates the resting-state functional connectivity of amygdala-related network in patients with generalized social anxiety disorder. BMC Psychiatry 16, 198.
Zhang, Y., Zhang, X., Zhang, J., et al., 2014. Gray matter volume abnormalities in type 2 diabetes mellitus with and without mild cognitive impairment. Neurosci. Lett. 562, 1–6.
Zhang, X.L., Fu, H.J., Yang, G.R., et al., 2018. The effects of cardiovascular risk factor combined anti-platelet therapy and the risk of cerebrovascular events in patients with T2DM in an urban community over 96-months follow-up: the Beijing communities diabetes study 19. Diabetes Res. Clin. Pract. 144, 236–244.
Zhou, X., Zhang, J., Chen, Y., et al., 2014. Aggravated cognitive and brain functional impairment in mild cognitive impairment patients with type 2 diabetes: a resting-state functional MRI study. J. Alzheimer's Dis. 41, 925–935.
Zhu, J., Zhuo, C., Xu, L., Liu, F., Qin, W., Yu, C., 2017. Altered coupling between resting-state cerebral blood flow and functional connectivity in schizophrenia. Schizophr. Bull. 43, 1363–1374.
Zhu, J., Zhu, D.M., Qian, Y., Li, X., Yu, Y., 2018. Altered spatial and temporal concordance among intrinsic brain activity measures in schizophrenia. J. Psychiatr. Res. 106, 91–98.
Zilliox, L.A., Chadrasekaran, K., Kwan, J.Y., Russell, J.W., 2016. Diabetes and cognitive impairment. Curr. Diabetes Rep. 16, 87.
Zuo, X.N., Ehmke, R., Mennes, M., et al., 2012. Network centrality in the human functional connectome. Cerebr. Cortex 22, 1862–1875.